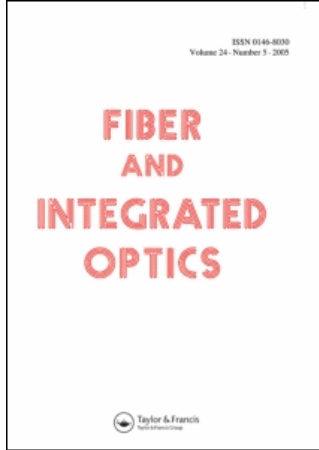


This article was downloaded by:[Ingenta Content Distribution TandF titles]
On: 11 June 2008
Access Details: [subscription number 791939330]
Publisher: Taylor & Francis
Informa Ltd Registered in England and Wales Registered Number: 1072954
Registered office: Mortimer House, 37-41 Mortimer Street, London W1T 3JH, UK



Fiber and Integrated Optics

Publication details, including instructions for authors and subscription information:
<http://www.informaworld.com/smpp/title~content=t713771194>

Optical Pulse Compression Schemes That Use Nonlinear Bragg Gratings

B. J. Eggleton; G. Lenz; N. M. Litchinitser

Online Publication Date: 01 October 2000

To cite this Article: Eggleton, B. J., Lenz, G. and Litchinitser, N. M. (2000) 'Optical Pulse Compression Schemes That Use Nonlinear Bragg Gratings', Fiber and Integrated Optics, 19:4, 383 — 421

To link to this article: DOI: 10.1080/014680300300001725
URL: <http://dx.doi.org/10.1080/014680300300001725>

PLEASE SCROLL DOWN FOR ARTICLE

Full terms and conditions of use: <http://www.informaworld.com/terms-and-conditions-of-access.pdf>

This article maybe used for research, teaching and private study purposes. Any substantial or systematic reproduction, re-distribution, re-selling, loan or sub-licensing, systematic supply or distribution in any form to anyone is expressly forbidden.

The publisher does not give any warranty express or implied or make any representation that the contents will be complete or accurate or up to date. The accuracy of any instructions, formulae and drug doses should be independently verified with primary sources. The publisher shall not be liable for any loss, actions, claims, proceedings, demand or costs or damages whatsoever or howsoever caused arising directly or indirectly in connection with or arising out of the use of this material.

Optical Pulse Compression Schemes That Use Nonlinear Bragg Gratings

B. J. EGGLETON
G. LENZ

Bell Laboratories
Lucent Technologies
Murray Hill, New Jersey, USA

N. M. LITCHINITSER

Institute of Optics
University of Rochester
Rochester, New York, USA

Nonlinear optical pulse compression of picosecond pulses typically requires long lengths of optical fiber and multiple components. Periodic structures, such as fiber Bragg gratings, are highly dispersive at wavelengths outside of the photonic bandgap. This implies that such gratings can be used as very short all-fiber compressors. In this paper a number of such compression schemes are reviewed involving uniform and nonuniform fiber Bragg gratings, relying on both soliton and nonsoliton compression principles. Experimental results supporting the corresponding underlying theory are also presented. Finally, an extension of one of the compression schemes is shown, which allows the generation of adjustable high-repetition rate soliton trains.

Keywords: optical pulse compression, fiber gratings, nonlinear optics, photonic bandgap structure, optical solitons, gap solitons, Bragg solitons

Sources that generate ultrashort optical pulses are valuable tools when experimentalists require femtosecond and picosecond time resolution, high peak powers, or large optical bandwidths [1]. Moreover, in telecommunication applications, pulses with shorter duration are needed as the per-channel capacity of communication systems increases beyond 100 Gb/s. At present, there are no electronic techniques that can produce 100 Gb/s electrical pulses, so short pulse optical sources are becoming a key technology. These optical sources require *optical pulse compressors* to achieve a wide range of functionality. They can reduce the pulse duration and increase the spectral bandwidth; they can generate pulse trains with adjustable repetition rate control; and when used in conjunction with optical regenerative amplifiers they can result in higher energy short pulses.

Received 28 April 1999; accepted 1 July 1999.

The authors acknowledge fruitful conversations with Dick Slusher, Martijn de Sterke, Prof. Govind Agrawal, Stefan Spalter, Paul Westbrook, and Geoff Burdge.

Address correspondence to Benjamin Eggleton, Bell Laboratories, Lucent Technologies, 600 Mountain Avenue, Room 1A-155, P. O. Box 636, Murray Hill, NJ 07974, USA. E-mail: egg@lucent.com

One such class of devices relies on the interaction of the Kerr nonlinearity and quadratic dispersion. These devices are inherently nonlinear and generate new bandwidth, an effect that purely linear devices are incapable of doing. This property, in turn, allows for the compression of transform-limited pulses into *shorter* transform-limited pulses; this should be contrasted with *dispersion compensation* devices, which recompress chirped pulses (i.e., not transform limited) into shorter pulses [2]. Furthermore, the interplay of self-phase modulation (SPM) with group velocity dispersion (GVD) can lead to solitons [3], which form the basis of various pulse compression and pulse generation schemes. These soliton and nonsoliton techniques are well-established, and have been used for many years [1]. Typically, the Kerr nonlinearity of optical fiber is used in conjunction with dispersion supplied by bulk devices, such as diffraction gratings, prisms, or an additional piece of fiber; in the case of optical solitons, the GVD and nonlinearity occur simultaneously in the optical fiber [1, 4].

In one scheme, first proposed by Tomlinson et al. [5], referred to here as a *Tomlinson compressor*, a fiber with positive dispersion, imposes a nearly linear, positive chirp on a pulse through the combined effect of SPM and positive GVD. In other words, SPM occurring in the optical fiber generates new frequencies in the pulse spectrum, and simultaneously the GVD linearizes the chirp and squares the pulse. The linear chirp on the pulse can then be compensated for by another dispersive element with negative GVD, such as a grating pair or a prism pair [5, 6], producing a nearly transform limited compressed pulse. This technique has been applied successfully to produce some of the shortest optical pulses reported [6].

Several pulse compression schemes have also been proposed that are based on soliton propagation, and in particular, rely on the robust nature of optical solitons. Mollenauer et al. [3] first proposed the *soliton-effect* compressor, which consists simply of a single piece of fiber with negative dispersion, whose length is suitably chosen. A transform limited pulse with appropriate peak intensity, propagating in this fiber, is compressed through the interplay between SPM and GVD [3, 4]. The compression is due to an initial narrowing phase that occurs during the evolution of a higher order soliton, before the initial soliton shape is restored after one soliton period [7]. The degree of compression is quite large although the compressed pulse is accompanied by a pedestal.

By varying the GVD along the direction of propagation in an optical fiber, Chernikov and Mamyshev have demonstrated the manipulation of a *fundamental* soliton resulting in *adiabatic* soliton compression of a transform limited pulse [8]. *Adiabatic soliton* compressors typically use a *dispersion profile* with monotonically decreasing GVD along the propagation direction. If the dispersion varies slowly enough, the soliton self-adjusts to maintain balance between GVD and nonlinearity, reducing its pulse width—hence the term adiabatic compression. This compression scheme is attractive because it inherently maintains the transform-limited characteristics of the pulse as it compresses, resulting in a clean pulse and avoiding any requirement for bulk optics. However, it can often require a complicated dispersion profile, requiring the splicing of different fiber sections or the addition of fiber with a tapered core.

In these various compression schemes, the relative strength of nonlinear and dispersive effects, which govern the compressor design, are given by characteristic length scales—namely, the dispersion length L_D and the nonlinear length L_{NL} , defined as follows [4]:

$$L_D = \frac{\sigma_0^2}{s^2 \beta_2}$$

$$L_{NL} = \frac{\lambda A_{eff}}{2\pi n_2 P} \quad (1)$$

Here, τ_0 is the full width at half maximum (FWHM); $\beta_2 = d^2\beta/d\omega^2$ is the GVD of the fiber; s^2 is a numerical factor that depends on the pulse shape (2.77 for Gaussian pulse and 3.11 for hyperbolic secant); λ is the wavelength; A_{eff} is the effective mode area; n_2 is the nonlinear refractive index of the fiber (which for standard fiber is $n_2 = 2.6 \times 10^{-16}$ cm²/W); and P is the peak power of the pulse. Note that in several of the techniques discussed in later sections, L_D and L_{NL} vary with position along the length fiber. The intrinsic GVD in standard optical fiber is very small (typically, $\beta_2 \sim -20$ ps²/km at communications wavelengths), which leads to long dispersion lengths. Thus the possibility of compact pulse compressors becomes difficult to realize. Furthermore, long fibers allow the various nonlinear effects, such as simulated Raman scattering (SRS), to impose limitations on the performance. It would be desirable to have a component that could introduce strong dispersion and which could be appropriately tailored.

Fiber Bragg gratings, and more generally any optical periodic structure (such as 2-dimensional or 3-dimensional photonic crystals), introduce high-reflectivity bands into the optical spectrum. Known as photonic band gap or stopbands, these bands are typically used as optical reflective filters [9]. When operated in transmission, at frequencies outside of the photonic bandgap they also possess a highly dispersive character—different wavelengths propagate with different velocities and are thus time-delayed by different amounts [10–12]. This dispersion becomes very large close to the edge of the photonic bandgap and can easily be 5–6 orders of magnitude larger than the dispersion of standard optical fiber. Increased GVD reduces the corresponding dispersion length from tens of kilometers to centimeters, and thus offers the possibility of compact pulse compressors. In order to exploit nonlinearities for nonlinear pulse compression, correspondingly higher peak powers are required when using standard fiber (i.e., the peak power available from standard Q-switched modelocked lasers) to achieve good compression [13]. Recent advances in chalcogenide fiber technology have led to fibers with Kerr nonlinearities that are two orders of magnitude larger than in standard fiber and fiber Bragg gratings in chalcogenide fibers were also demonstrated [14]. This strong dispersion that exists in Bragg gratings and the ability to fabricate gratings with an almost arbitrary index profile, and thus arbitrary dispersion profile, potentially in highly nonlinear fibers, will result in very small, flexible, and simple compression devices with low peak power requirements.

In this paper a comprehensive review of optical pulse compression techniques is presented that use nonlinear Bragg grating structures. The pulse compressors and generators that are reviewed here are based on apodized fiber Bragg gratings and operate in *transmission*. That is, the optical pulses propagate outside of the photonic bandgap and utilize the strong GVD, which is present even at wavelengths far removed from the photonic bandgap. In doing so, one restricts oneself to fiber geometries and Kerr-type nonlinearities. Although many of the concepts discussed can be applied more generally in other cases (e.g., photonic band gap structures (see, for example, [15]), or cascaded χ_2 nonlinearities as an effective Kerr medium (see, for example, [16])).

It is shown that by utilizing the strong GVD of Bragg gratings, compact, efficient pulse compressors are realizable. This analysis is based on an approximate model using a nonlinear Schrödinger equation (NLSE), which is valid for frequencies outside of the photonic band gap of a grating and sufficiently removed from the photonic band gap edge. Thus, one does not consider the case in which the frequency spectrum is confined partially within the band gap [17].

The remainder of this paper discusses dispersion in Bragg gratings and pulse compression schemes in four additional sections followed by a discussion of the results. In the second section GVD in Bragg grating structures is reviewed and analytic results describing GVD and higher order dispersion are presented. A figure of merit (FOM) is also introduced that quantifies how constant the GVD is over the pulse bandwidth, and it is shown that this is critical in the design and analysis of pulse compressors based on fiber gratings. Then nonlinear pulse

propagation in Bragg gratings is considered, establishing an NLSE description, and some important results of this description are presented. Also briefly discussed are the properties of Bragg solitons, which are pulses that can propagate through a grating, without changing shape, in spite of the strong GVD; they represent a balance between the strong GVD introduced by the grating and SPM. They underlie several of the pulse compression schemes discussed in this paper. In the third through sixth sections the various optical pulse compression schemes are presented.

In the third section, a *Bragg grating compressor* is described that relies only on the GVD of the grating in order to compress a pulse, which is spectrally broadened and chirped due to SPM in a separate nonlinear medium. Experimental results show compression of 80 ps pulses generated by a Q-switched modelocked Nd:YLF laser to 15 ps pulses using a 6 cm apodized fiber Bragg grating [18]. The degree of compression in this case can be large, but the quality is not perfect due to the nonlinear chirp associated with SPM.

In the fourth section, the *Tomlinson Bragg grating compressor* is presented, a pulse compression scheme that utilizes both the strong GVD and the Kerr nonlinearity occurring in a fiber Bragg grating [19]. Based on a two-section device similar in principle to the Tomlinson compressor [5], it uses a Bragg grating to increase the bandwidth and simultaneously linearize the resulting chirp of a pulse. The second linear section, which can also be a grating, acts as a chirp compensator (i.e., removes the mostly linear chirp). Due to the combined effect of the SPM and positive GVD the chirp is almost linear and thus the resulting pulse is clean.

In the fifth section, the recent experimental results on nonlinear pulse compression and Bragg soliton propagation in fiber gratings are reviewed. It is shown that experimental results are in good agreement with both numerical simulations of the nonlinear coupled mode equations (NLCME) and the NLSE. The nonlinear pulse compression occurs because of *soliton-effect* compression, where the GVD is provided by a Bragg grating. The *Bragg soliton-effect compressor* requires only a single apodized Bragg grating; however, the compressed pulse is accompanied by a pedestal.

In the sixth section, a novel pulse compression scheme is presented that relies on the propagation of Bragg solitons in a *nonuniform* fiber Bragg grating [20]. The *Adiabatic Bragg soliton compressor* scheme is based on adiabatic soliton compression using a *nonuniform* grating in which the dispersion decreases along the grating. This technique has the advantage that it only requires one component (i.e., one grating) and produces a clean nearly transform limited pulse. The NLSE model for nonlinear pulse propagation in Bragg gratings, introduced in the second section, is extended to treat nonlinear pulse propagation in *nonuniform* Bragg gratings and is used to design a compact adiabatic Bragg grating compressor. These results are then generalized and a high repetition rate optical pulse train source based on the beating together of two CW sources is presented. By sending them through a grating, one transforms the beat signal into a train of fundamental solitons with the repetition rate determined by the frequency separation of the CW sources. In the final section concluding remarks are offered and possible future directions for this work are considered.

Background

Bragg Reflection

A one-dimensional photonic crystal is considered, such as a Bragg grating, located in the core of an optical fiber, whose axis is in the z -direction. The linear refractive index is given by

$$n(z) = n_0 + \delta n(z) + \Delta n(z) \cos\left(\frac{2\pi}{\Lambda} z + \Phi(z)\right), \quad (2)$$

where n_0 is the refractive index of the fiber core, $\delta n(z)$ is the change in the average refractive index, $\Delta n(z)$ is the refractive index modulation depth, Λ is the grating period, and $\Phi(z)$ is the phase that allows for grating period variations. For typical gratings in optical fiber, $n_0 \sim 1.5$, both $\Delta n(z)$ and $\delta n(z)$ can be as large as 0.01 in H_2 loaded fibers [9], and the period is usually of the order of $\Lambda \sim 0.5 \mu\text{m}$. All of the gratings, referred to throughout this work, rely on the mechanisms of photosensitivity in germanosilicate glass [9].

Uniform Bragg gratings are well understood. If the wavelength of the incident light is close to the resonant Bragg wavelength of the periodic grating structure then light will be strongly reflected. For a grating with a period Λ , the Bragg wavelength is

$$\lambda_B = 2\bar{n}\Lambda, \quad (3)$$

where $\bar{n} = n_0 + \delta n$. The width $\Delta\lambda$ of the band of wavelengths that are strongly reflected by the grating, referred to as the “*photonic band gap*,” is

$$\frac{\Delta\lambda}{\lambda_B} \cong \frac{\Delta n}{n}. \quad (4)$$

If the wavelength of the incident light lies within the photonic band gap, the field envelopes in the grating are evanescent and light is mostly reflected, while outside the photonic band gap, the fields are propagating waves and light is mostly transmitted.

In a grating with a uniform index modulation, spectral sidelobes are present in the transmission spectrum for wavelengths outside of the photonic band gap (i.e., in the passband). These sidelobes are accompanied by distortion, in the form of ripple in the GVD of the grating [52]. They result from a mismatch in the effective index of the grating and the surrounding medium (i.e., bare fiber), and can be removed by allowing the index modulation to vanish smoothly at each end, a process known as apodization [27]. This technique is widely exploited in designing photonic components for wavelength division multiplexing applications in which the out-of-band reflections are highly undesirable [21, 22]. Apodization is also critical in the design and implementation of fiber grating-based pulse compressors, which are considered here.

Apodized gratings are just one example of nonuniform Bragg gratings in which one or more of the quantities, $\delta n(z)$, $\Delta n(z)$, and $\Phi(z)$, are slowly varying functions along the length of the grating. Light propagation in this case can be conveniently described using a *reflection-band diagram* [23], which is used throughout this paper to the various pulse compression schemes. Figure 1 shows examples of such diagrams for various nonuniform gratings: Figure 1a represents a uniform grating with constant index modulation; b represents a linearly tapered fiber grating with an index modulation that varies linearly along the length of the grating (constant average refractive index); and c represents an apodized grating with the index modulation vanishing smoothly at each of the grating (constant average refractive index). Each point on the horizontal axis of the diagram corresponds to a particular point along the grating with a specific detuning. The shaded region corresponds to those frequencies that are strongly reflected, whereas the frequencies in the clear region are transmitted.

Gratings are often fabricated in photosensitive fiber using the phase mask scanning technique [21, 24, 25], in which an ultraviolet beam (with a wavelength of typically 242–248 nm) is scanned along the length of the phase mask. Gratings as long as 1 meter have been fabricated using this method [26]. Fabrication of apodized gratings, in which the grating amplitude varies along the length of the grating, involve a two-step procedure [21]. First, an ultraviolet beam is scanned along the length of the phase mask. The intensity of the ultraviolet beam is varied as the beam is scanned along the axis of the fiber creating the modulated component

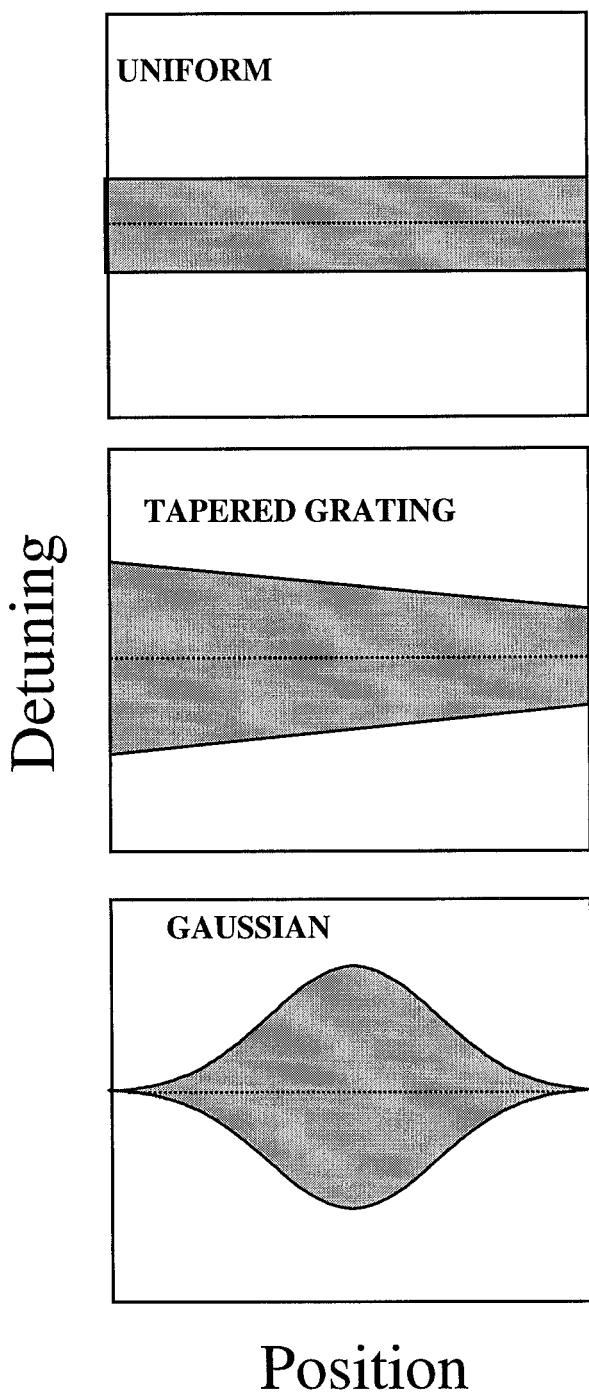


Figure 1. Schematic reflection band diagrams illustrating light propagation through Bragg gratings: (a) uniform Bragg gratings, (b) linearly tapered fiber Bragg gratings, and (c) apodized fiber Bragg gratings. The horizontal axis is positioned along the length of the grating and the vertical axis is detuning.

of the grating. Second, the unmodulated component of the grating is then imprinted in the same manner without the phase mask present. This two-step technique ensures that the average refractive index of the grating remains approximately constant along the length of the grating even though its strength changes, minimizing sidelobes. To a good approximation the apodization profiles discussed in this work are Gaussian functions as illustrated in Figure 1c [22, 27].

Bragg Grating Dispersion

Nonlinear pulse propagation in Bragg gratings can be described using the NLCMEs, which are believed to be the most accurate description of nonlinear pulse dynamics in Bragg gratings [28]. These equations are valid only for shallow gratings ($\Delta n \ll \bar{n}$) and for wavelengths close to the Bragg wavelength. At high intensities the nonlinearity becomes important and thus one needs to include the intensity dependent refractive index,

$$n = n_L + n_2 I, \tag{5}$$

where $I = P/A_{eff}$ is the peak intensity.

The NLCMEs can be derived by substituting the Ansatz for the electric field E , [28],

$$E(z, t) = [E_+(z, t)e^{+ik_B z} + E_-(z, t)e^{-ik_B z}]e^{-i\omega_B t} + c.c., \tag{6}$$

which is assumed to be linearly polarized, into Maxwell’s wave equation and by making use of the fact that the field envelopes are slowly varying. Here, $k_B = \pi/\Lambda$ and $\omega_B = \pi c/(\bar{n}\Lambda)$ are the wave number and the frequency at the Bragg condition, respectively, and E_+ and E_- are the slowly varying field envelope amplitudes of forward and backward propagating waves. The resulting NLCMEs for E_{\pm} can be written as [28]:

$$\begin{aligned} i \frac{\partial E_+}{\partial z} + i \frac{1}{V} \frac{\partial E_+}{\partial t} + \kappa(z)E_- + \Gamma_S |E_+|^2 E_+ + 2\Gamma_{\times} |E_-|^2 E_+ &= 0 \\ i \frac{\partial E_-}{\partial z} + i \frac{1}{V} \frac{\partial E_-}{\partial t} + \kappa(z)E_+ + \Gamma_S |E_-|^2 E_- + 2\Gamma_{\times} |E_+|^2 E_- &= 0 \end{aligned} \tag{7}$$

Here $V = c/\bar{n}$ is the phase velocity of light in fiber, where c is the speed of light;

$$\kappa(z) = \frac{\pi \Delta n(z) \eta}{\lambda_B} \tag{8}$$

is the coupling coefficient, which is allowed to vary along the length of the grating, and $\eta \sim 0.8$ is the fraction of the total energy in the fiber core. Γ_S and Γ_{\times} are the nonlinear parameters responsible for self- and cross-phase modulation such that $\Gamma_S = \Gamma_{\times} = 2\pi n_2/\lambda_B$.

Linear pulse propagation through gratings can be understood using the linearized coupled mode equations, where $\Gamma_{\times} = \Gamma_S = 0$. One needs to consider the dispersion relation $\omega(k)$, which is also the relationship between the frequency detuning parameter

$$\delta = \frac{1}{V} (\omega - \omega_B) \tag{9}$$

and the propagation constant $\beta = k - k_B$, where ω and k are the optical frequency and the propagation wavenumber, respectively. For an infinite uniform grating the dispersion relation can

be obtained from the linearized NLCME eqs. (7) by insertion of a plane-wave solution of the form

$$E_{\pm} = C_{\pm} \exp[i(\beta z - V\delta t)], \quad (10)$$

where C_{\pm} are constants. This substitution yields the dispersion relation

$$\delta = \pm \sqrt{\kappa^2 + \beta^2}, \quad (11)$$

which is illustrated in Figure 2, for both a uniform medium (dashed lines) and a periodic medium (solid lines). Figure 2 shows that for frequencies in the range $-\kappa \leq \delta \leq \kappa$, defining the photonic band gap, no propagating solutions are allowed; this corresponds to the regions of high reflectivity. Light can propagate outside this region, which corresponds to the pass-band.

The slope of the dispersion curve $d\delta/d\beta$ gives the group velocity, while the curvature, $d^2\delta/d\beta^2$, gives the GVD. In the absence of the grating, light propagates at the speed of light in the medium (one ignores the background material dispersion, as it is negligible over the bandwidth under consideration). In the presence of the grating, the group velocity vanishes at the band edge and asymptotically approaches the speed of light in the medium far from the Bragg resonance. The reduction in the group velocity can be explained in terms of the multiple Fresnel reflections that occur at each of the individual grating rulings, resulting in additional path length. This extreme variation in the group velocity over such a relatively small range of wavelengths (roughly equal to the bandwidth of the grating) leads to strong GVD.

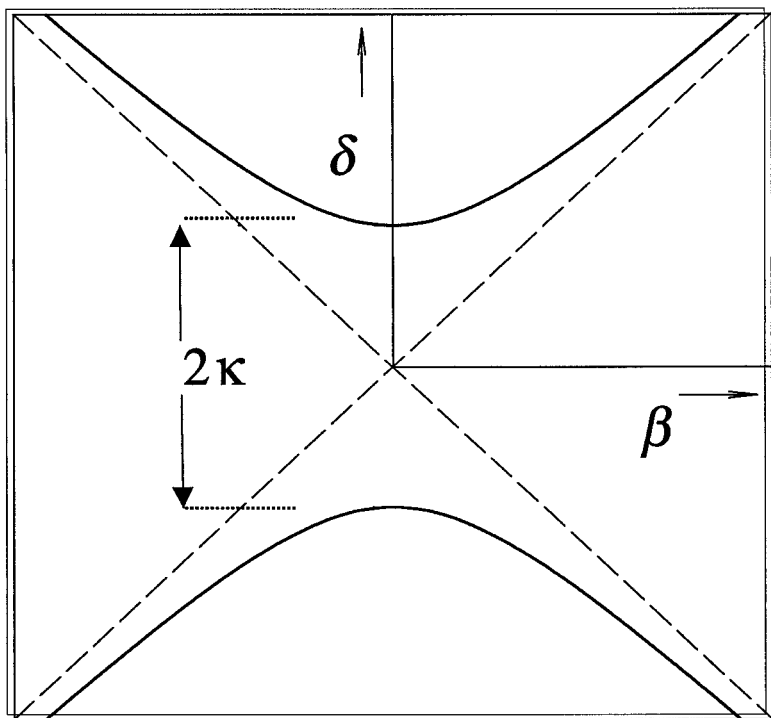


Figure 2. Dispersion relation of uniform Bragg grating. The vertical axis is the detuning parameter and the horizontal axis is the propagation constant.

Indeed, it has been shown that the grating GVD can be up to six orders of magnitude larger than that of standard telecommunication fiber [11].

On the long-wavelength side of the band gap ($\delta < -\kappa$), the grating GVD is positive, and can be used to compensate for the negative dispersion effects which are caused by propagation in optical fiber at communication wavelengths [11]. On the short-wavelength side of the photonic band gap ($\delta > \kappa$), the grating GVD is negative and solitons are supported [13, 29]. At frequencies close to the edge of the photonic band gap the grating also exhibits significant higher-order dispersion, which affects the light propagation [10, 12]. The effect of this grating dispersion can be accounted for mathematically by expanding the propagation constant $\beta(\omega)$ in a Taylor series [12, 30]

$$\beta(\omega) = \beta_0 + \beta_1(\omega - \omega_0) + \frac{1}{2}\beta_2(\omega - \omega_0)^2 + \frac{1}{6}\beta_3(\omega - \omega_0)^3 + \dots, \quad (12)$$

where β_n is the n th derivative of β with respect to ω . Each term in this series has physical significance, which is discussed below. The group velocity can be calculated by $v_g \sim d\omega/dk = Vd\delta/d\beta$, which gives

$$v_g = \pm V\sqrt{1 - (\kappa/\delta)^2}. \quad (13)$$

To quantify the GVD inside the grating, one considers the second term in the Taylor series expansion of the propagation constant [10, 12, 30]

$$\beta_2 = -\left(\frac{1}{V}\right)^2 \frac{1}{\delta} \frac{\left(\frac{\kappa}{\delta}\right)^2}{\left(1 - \left(\frac{\kappa}{\delta}\right)^2\right)^{3/2}}, \quad (14)$$

which is illustrated in Figure 3 by the solid line; the dashed line represents the edges of the photonic band gap. The GVD is frequency-dependent and, therefore, is not constant over the spectral bandwidth of a short pulse. Thus the third-order dispersion, which is the next term in the Taylor series expansion, becomes

$$\beta_3 = 3\left(\frac{1}{V}\right)^3 \frac{1}{\delta^2} \frac{\left(\frac{\kappa}{\delta}\right)^2}{\left(1 - \left(\frac{\kappa}{\delta}\right)^2\right)^{5/2}}, \quad (15)$$

and should not, in general, be neglected. For example, consider a typical fiber grating with $\kappa = 10 \text{ cm}^{-1}$ and a pulse with duration $\tau_0 = 10 \text{ ps}$, a detuning of $\delta = 15 \text{ cm}^{-1}$, corresponding to $v_g = 0.7 V$; then the dispersion length is $L_D^{(2)} \sim 0.5 \text{ cm}$, while the dispersion length for third-order dispersion is $L_D^{(3)} = \tau_0^3/\beta_3 \sim 0.3 \text{ cm}$. Note also that in a grating, the third-order dispersion is always positive regardless of the sign of δ . This should be compared with propagation in standard communications optical fiber in which the dispersion length for a 10 ps pulse at $1.5 \text{ }\mu\text{m}$ is 4 km and the length for third-order dispersion is $L_D^{(3)} = 10,000 \text{ km}$.

Because third-order GVD distorts short optical pulses, the ratio between the third and second-order dispersion terms, often defined as the FOM for characterizing the performance of a fiber grating, can be expressed as [30]

$$F = \frac{|\beta_2|}{|\beta_3|} \alpha_0 = V\alpha_0 \frac{\delta^2 - \kappa^2}{3\delta}. \quad (16)$$

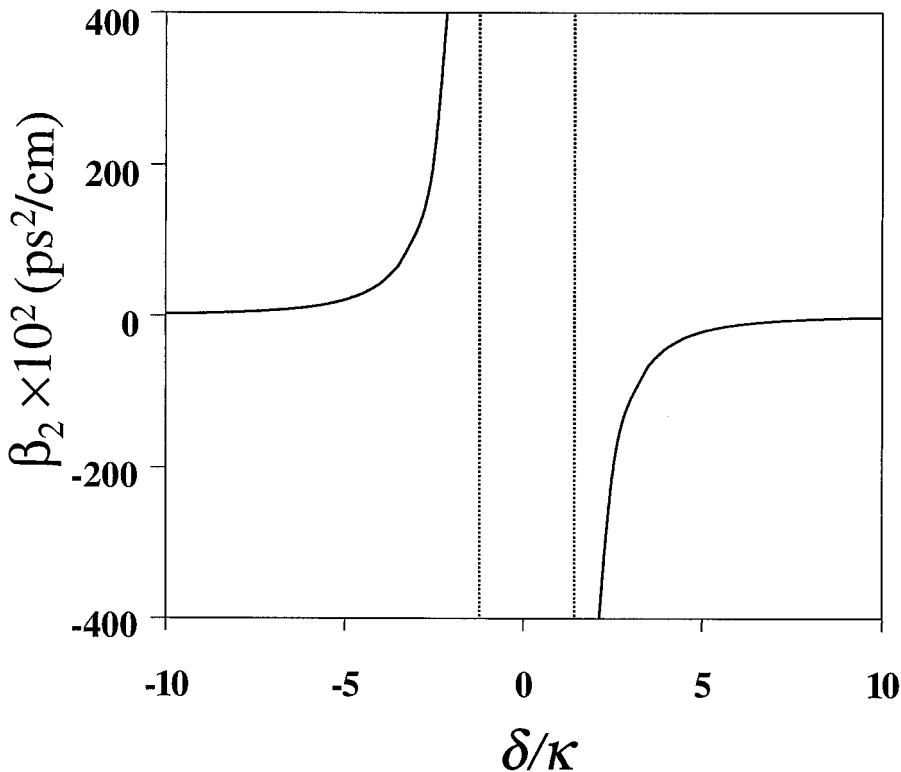


Figure 3. Quadratic dispersion of Bragg grating versus detuning. The dashed line represents the edges of the photonic band gap.

Clearly, to minimize the detrimental effects of third-order dispersion, F must be as large as possible, i.e. $F \gg 1$. Using this FOM, the grating-based pulse compressors were designed as described in a later section.

Bragg Solitons in the Nonlinear Schrödinger Limit

As discussed in the previous section, in general, the propagation through a fiber grating is described by a set of NLCME. However, if the grating quadratic dispersion is nearly constant over the spectral bandwidth of the pulse (i.e., $F \gg 1$) and the intensity of light is sufficiently low so that $\Delta n_{NL} \ll \Delta n_L$, then these equations can be reduced to a simple NLSE having the form [28, 29, 31, 32]

$$i \frac{\partial A}{\partial z} - \frac{\beta_2}{2} \frac{\partial^2 A}{\partial \sigma^2} + \Gamma |A|^2 A = 0. \quad (17)$$

Here A is an envelope function that modulates the eigenfunctions or Bloch waves associated with the grating. β_2 is the GVD of the grating given by eq. (14), and Γ is the effective nonlinear coefficient (given below). Both of these quantities are assumed to be axially uniform for now. Finally, $\tau = t - z/v_g$ is the reduced time. The parameter Γ is frequency-dependent inside the grating and is related to the grating parameters through the relation [29]

$$\Gamma = \frac{2\pi}{\lambda} n_2 \frac{1 + \kappa^2/(2\delta^2)}{\sqrt{1 - \kappa^2/\delta^2}}. \tag{18}$$

The derivation of eq. (17)–(18) is based on a multiple scales approach and has been presented elsewhere (see [28] for a complete derivation).

It is noted that close to the edge of the photonic band gap (i.e., $\kappa \sim \delta$), the intensity inside the grating is enhanced with respect to that outside of the grating; this is the reason for the additional factor in eq. (18). This can be attributed to both the standing wave field inside the grating and the reduced group velocity of light inside the grating [31]. In addition to this, eq. (17) describes nonlinear pulse propagation inside the Bragg grating and ignores the “coupling problem.” One thus needs to relate the incoming field, i.e., the pulse incident upon the grating, to the field just inside the grating at which point eq. (17) applies. If one assumes that the grating is suitably apodized, then the reflectivity outside of the photonic band gap is negligible, and one can show to a good approximation, that the total field intensity inside the grating is enhanced by a factor of V/v_g , so that $I_{in} = (V/v_g)I_{out}$ [29]; this approximation neglects propagation in the apodized regions. Combining these two effects can result in enhancements in the nonlinearity as high as 3–5 in typical fiber grating experiments [29]. Finally, it is noted that in a nonuniform Bragg grating such as that described in a previous section, the coefficients in eq. (17) can vary along the length of the grating. This point is returned to later.

This approximate description is a very valuable tool in understanding nonlinear pulse propagation through Bragg gratings. This approach highlights the physics and leads to results that are in good agreement with both NLCME and experimental results, as discussed in a later section. A very interesting consequence of this equation is a new kind of soliton, referred to as a *Bragg soliton* [13, 29, 31, 33, 34], which relies on the GVD provided by the Bragg grating rather than on material dispersion [13].

Bragg solitons, as described by the NLSE, represent a special case of more general solitary wave solution found by Aceves and Wabnitz [35]; this is returned below. The fundamental Bragg soliton, in the NLSE limit, can now be written as [4]

$$A(\sigma) = \sqrt{\left| \frac{\beta_2}{\Gamma} \right|} \frac{1}{\sigma_0} \operatorname{sech}(\sigma/\sigma_0). \tag{19}$$

By definition, the electric field envelope A for a Bragg soliton obeys the following relation [36]:

$$N^2 = \frac{L_D}{L_{NL}} = \frac{\sigma_0^2}{\beta_2} \Gamma I_{in} = \frac{E_s \Gamma}{2A_{eff}} \frac{\sigma_0}{|\beta_2|}, \tag{20}$$

where N —an integer—is the Bragg soliton order and Γ is defined in eq. (18). The peak intensity of the pulse inside the grating is then $I_{in} = |A|^2$, where τ_0 is the pulse width and $ES = 2I_{in}\tau_0 A_{eff}$ is the soliton energy. One can now apply the standard NLSE results for a soliton in uniform media, and by relating the fields outside and inside the grating, one finds that the peak intensity required for launching a $N = 1$ Bragg soliton is [29]

$$I_{out} = \frac{1}{V^2} \frac{\lambda \kappa^2}{\pi \sigma_0^2 (2\delta^2 + \kappa^2)(\delta^2 - \kappa^2)^{1/2} n_2}. \tag{21}$$

An interesting property of solitons is that the solution $A(\tau)$ is periodic with a period of Z_0 , given by [4]

$$z_0 = \frac{\pi \alpha_0^2}{2|\beta_2|} = \frac{\pi}{2} \alpha_0^2 V^2 \frac{(\delta^2 - \kappa^2)^{3/2}}{\kappa^2}. \quad (22)$$

This periodicity is obeyed by all higher order solitons ($N \geq 2$). In fact, during the evolution of a higher order soliton over one soliton period, it first contracts to a fraction of its initial width, splits into distinct pulses, and then merges again, recovering the original shape at the end of the soliton period. The initial compression is often referred to as *soliton-effect* compression and forms the basis of a well-known pulse compression scheme [3]. Recent experimental results studying soliton-effect pulse compression in fiber Bragg gratings are reviewed in a later section.

There are some major differences between Bragg solitons and conventional solitons that are briefly reviewed here:

- Bragg solitons can, in principle, travel at any velocity between 0 and V . In experiments, velocities as low as $0.5 V$ have been reported [29]. In nonuniform Bragg gratings, the velocity varies along the length of the grating.
- The GVD is caused by the presence of the grating and not by the inherent material dispersion of glass. The magnitude of the grating GVD can be up to 5–6 orders of magnitude larger than the material dispersion of glass. Thus the soliton period, which is proportional to L_D , is correspondingly smaller.
- The magnitude of the nonlinear coefficient in the NLSE can exceed that in conventional fiber and is strongly frequency-dependent close to the edges of the photonic band gap.
- Bragg solitons represent solutions to the NLCME which are a set of nonintegrable equations [35]. These solitary wave solutions are known to reduce to the NLSE solutions given by eq. (19) in the appropriate limit [32]. Since these solitary waves are solutions to the full NLCME, they include all orders of dispersion and their existence is not restricted to the regimes of good FOM as given by eq. (16).

Using Linear Properties of Bragg Gratings for Optical Pulse Compression

Principle of Operation

In this section, results of a compression scheme are presented in which spectrally broadened 80 ps (FWHM) pulses, generated by a modelocked/Q-switched YLF laser, are compressed down to 15 ps, using an unchirped, apodized Bragg grating operating in transmission. In this example, the propagation through the Bragg grating is linear (i.e., the power is low enough such that L_{NL} is very large and the effects of nonlinearity in the grating can be neglected) [18]. The compression factor of 5 is in good agreement with theory and numerical simulations, and is close to the compression that could have been achieved with an ideal compressor.

The key to this compression scheme, which is illustrated in Figure 4, is that an intense pulse propagating through a nonlinear medium spectrally broadens and acquires a frequency sweep. In this case, the nonlinear medium is the laser rod of the Nd:YLF laser [37, 38] operating in Q-switched modelocked mode. In such lasers, the high intensities of the modelocked pulses under the Q-switch envelope in the cavity can develop significant SPM. Different modelocked pulses under the Q-switched envelope will have different intensities and thus acquire nonlinear phase shifts of different magnitudes. In contrast to the chirp acquired by a linear pulse propagating in a dispersive medium, the chirp is intensity dependent and is approximately linear only over the central portion of the pulse. The spectrally broadened pulse can

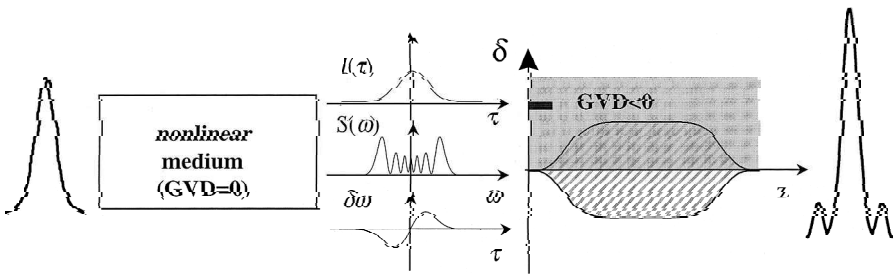


Figure 4. Schematic of linear Bragg grating compressor. The first section is for bandwidth generation and the second section is for chirp compensation. The Bragg grating is a purely linear device incapable of compensating for the nonlinear chirp.

then be compressed using a dispersive element (such as a linear Bragg grating), which exhibits negative dispersion [4]. This compression is not perfect because of the residual noncompressible nonlinear chirp. In addition, for nonlinear phase shifts of $\Delta\phi \geq 3/2\pi$, zeros are introduced in the spectrum, which cannot be restored by any linear system.

Analysis

Consider a Gaussian pulse with a (1/e) halfwidth of τ_0 , which is chirped by SPM and let $\Delta\phi = (2\pi/\lambda)n_2IL$ denote the peak intensity induced phase shift, where λ is the free space wavelength and L is the optical path length. The necessary GVD for optimum pulse compression can be shown to be [18, 36]

$$|\beta_2|z \approx \frac{\sigma_0^2}{2\Delta\phi}, \tag{23}$$

where β_2 is the value of the GVD in units of ps^2/cm and z is the length of the grating in units of cm. For large nonlinear phase shifts ($\Delta\phi > 2$), the resulting compression ratio can then be approximated by [18]

$$C = \tau_0/\tau_c \approx 0.75\Delta\phi, \tag{24}$$

where τ_c is the duration of the compressed pulse. Ultimately, the quality of compression is limited by the bandwidth over which the dispersion is constant.

Pulse Compression Results

The parameters required for pulse compression of a spectrally broadened pulse are now examined using an apodized (unchirped) fiber grating. Consider a Gaussian pulse with 80 ps (FWHM), spectrally broadened by propagation through a nonlinear medium with a maximum nonlinear phase shift of $\Delta\phi = 7$. From eq. (24) one would expect a compression factor of $C = 5.25$ that is limited by residual nonlinear chirp and the higher order dispersion of the grating. One considers a grating in which $\kappa = 21.5 \text{ cm}^{-1}$ with a total length of 6.5 cm. The grating is also suitably apodized; the effective length of the apodized regions is approximately 0.75 cm, which is sufficiently small to be ignored in this analysis. Using eq. (23) and the length of the

grating, one determines that the dispersion of the grating should be $\beta_2 = -33 \text{ ps}^2/\text{cm}$. One can now solve eq. (14) to find the detuning parameter that gives maximum compression, giving $\delta = 39.0 \text{ cm}^{-1}$ ($\Delta\lambda = -0.47 \text{ nm}$). Note that this corresponds to the short wavelength side of the photonic bandgap (negative dispersion).

Figure 5 shows the numerically simulated compression for the above example. The dotted line shows the input spectrally broadened pulse ($\tau_0 = 80 \text{ ps}$) and the solid line shows the pulse upon transmission through the grating. The transmitted pulse is compressed to a width of approximately 15 ps, representing a compression factor of $C \cong 5.2$, which is in good agreement with that predicted from eq. (24). Note that the structure on the trailing edge of the compressed pulse, which contains approximately 10–15% of the energy in the entire pulse. It is not surprising that the compression is not perfect because in this example the FOM given by eq. (16) is $F \cong 3$, and thus the third-order dispersion is still significant [12]. The dashed line in Figure 5 shows the calculated compression pulse obtained by assuming only quadratic dispersion in the compressor. Because of the nonlinear nature of the chirp associated with SPM, the pulse is not entirely compressed, even in the case of the ideal quadratic compressor.

The transmission spectrum of an apodized fiber Bragg grating is shown in Figure 6 as a function of detuning from the center of the photonic band gap. The photonic band gap is approximately 0.50 nm wide, corresponding to $\kappa = 21.5 \text{ cm}^{-1}$ with a total length of 6.5 cm, including 0.75 cm apodized regions on each end of the grating. The uniform region of the grating is thus 5 cm long.

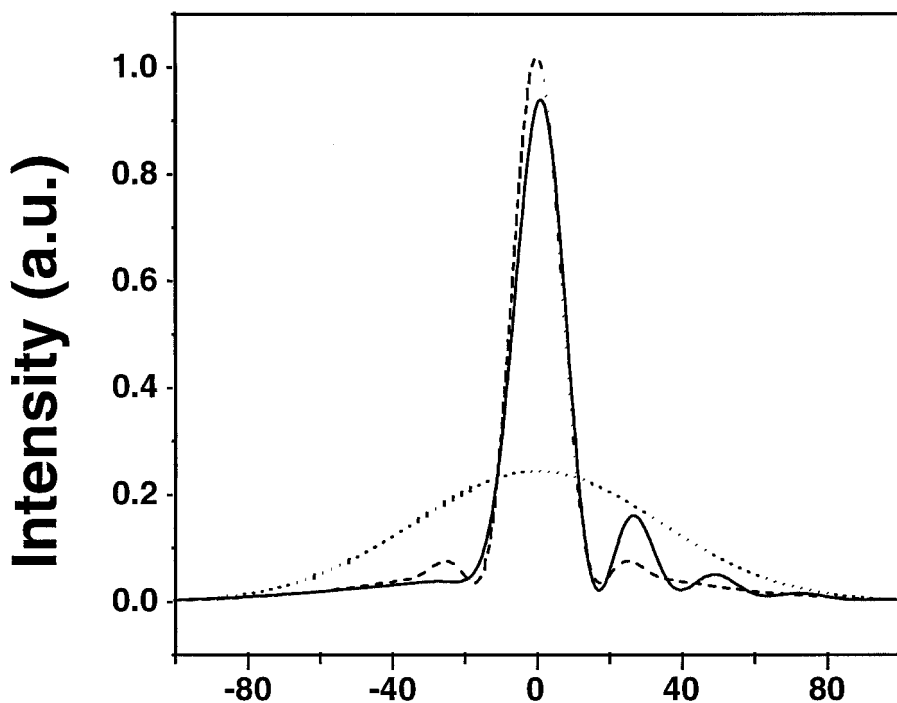


Figure 5. Pulse compression according to numerical simulation of NLCME. Grating parameters: $\kappa = 21.5 \text{ cm}^{-1}$ and $L = 0.5 \text{ cm}$ (apodized). Short-dashed curve is spectrally broadened input pulse ($\tau = 80 \text{ ps}$, $\Delta\phi = 7$, $\delta = 39 \text{ cm}^{-1}$, $\Delta\lambda = -0.47 \text{ nm}$), solid curve is pulse compressed by the grating, and dashed curve is pulse compressed by an ideal compressor with only quadratic dispersion.

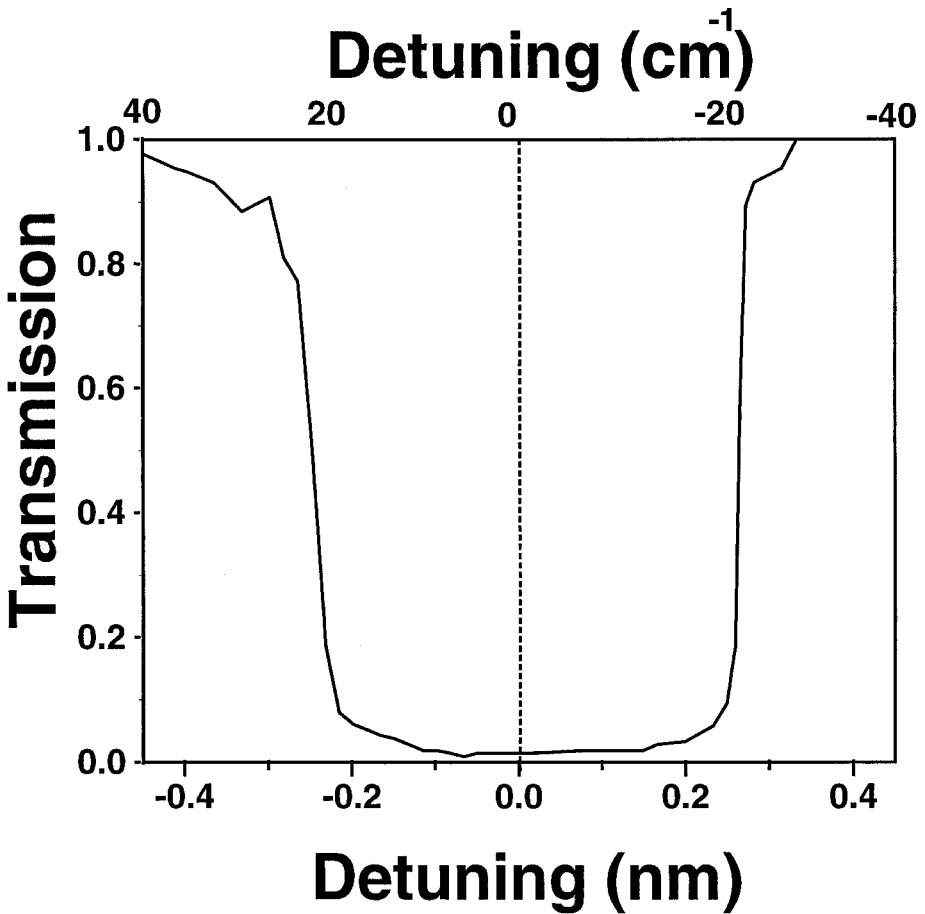


Figure 6. Measured transmission spectrum of apodized Bragg grating as a function of detuning: wavelength (bottom axis) and frequency detuning (top axis).

Figure 7 shows a typical experimental result of the compression using the apodized fiber grating as a transmissive dispersive element. In this example, one estimates that the nonlinear phase shift is $\Delta\phi = 7$. This shift corresponds to a pulse close to the peak of the Q-switched train where the nonlinear phase shift is largest [18]. The detuning of the input pulse is adjusted to maximize the compression, where the detuning is $\Delta\lambda = -0.45 \text{ nm}$ ($\delta = 38 \text{ cm}^{-1}$), corresponding approximately to the parameters in Figure 5. The dashed line represents the input pulse with a width of 80 ps, and the solid line represents the compressed pulse having a measured width of 25 ps. Since the detection system has a total response time of 20 ps, one concludes that the compressed pulsewidth is approximately 15 ps, representing a compression factor of greater than 5 in good agreement with numerical simulations. Note that there is some structure on the trailing edge containing approximately 15–20% of the energy of the entire pulse. This structure is clearly associated with higher order dispersion in the grating and nonlinear chirp.

Figure 8 shows the measured deconvolved pulsewidth (FWHM) for a fixed nonlinear phase shift of $\Delta\phi = 7$ as one varies the detuning of the input pulse. At detunings far from the

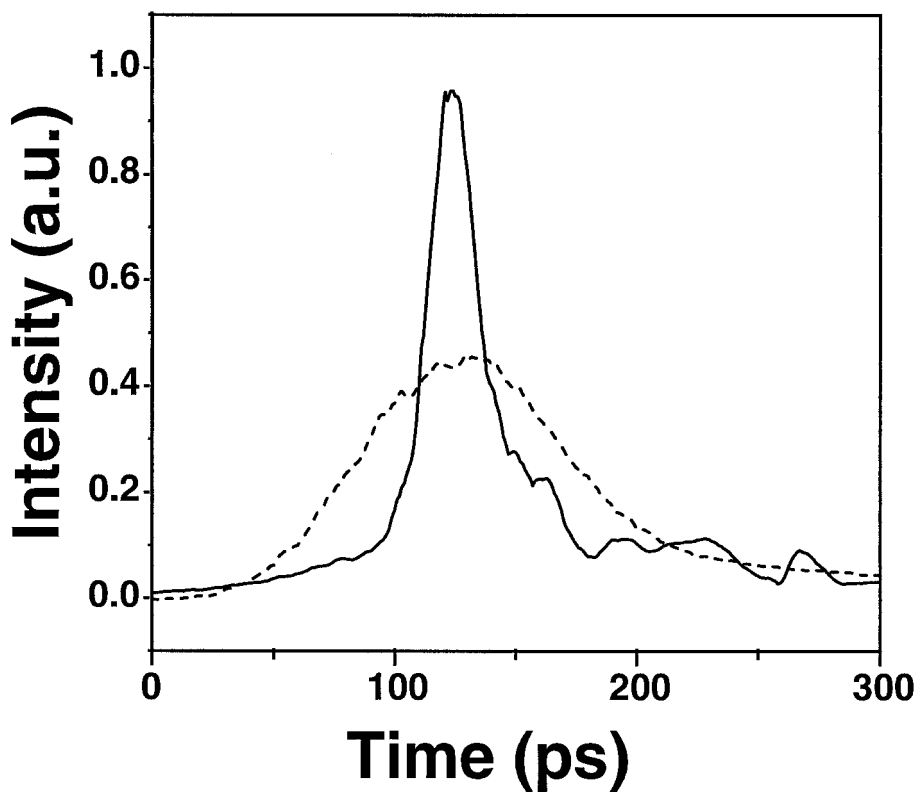


Figure 7. Experimentally measured transmitted intensity as a function of time. Dashed curve is the spectrally broadened pulse ($\tau = 80$ ps, $\Delta\phi = 7$, $\Delta\lambda = 0.45$ nm) and the solid curve is the compressed pulse.

photonic band gap, the dispersion is small and the pulse shape is mostly unaffected. The transmitted pulse reaches a minimum pulsewidth for a detuning of $\Delta\lambda = -0.45$ nm ($\delta = 38$ cm⁻¹), which corresponds to the case shown in Figure 7. Close to the edge of the photonic band gap, the dispersion overcompensates the spectrally broadened pulse and higher order dispersion becomes significant.

The effects of varying the amounts of spectral broadening was also investigated. This was achieved experimentally by selecting different pulses in the Q-switched train. Figure 9 shows the deconvolved pulsewidth (FWHM) of the transmitted pulse for different values of the estimated nonlinear phase shift in the laser cavity. In this example, the detuning is fixed to $\Delta\lambda = -0.45$ nm ($\delta = 38.0$ cm⁻¹) from the center of the photonic band gap. It is worth noting that for nonlinear phase shifts of $\Delta\phi < 0.2$, the transmitted pulse is mostly unaffected. The regime corresponds roughly to the experiments described in a later section.

Discussion

The pulse compression achievable using this scheme is not perfect because of the nonlinear chirp and the higher order dispersion of the grating. The quality of the compression can be improved by:

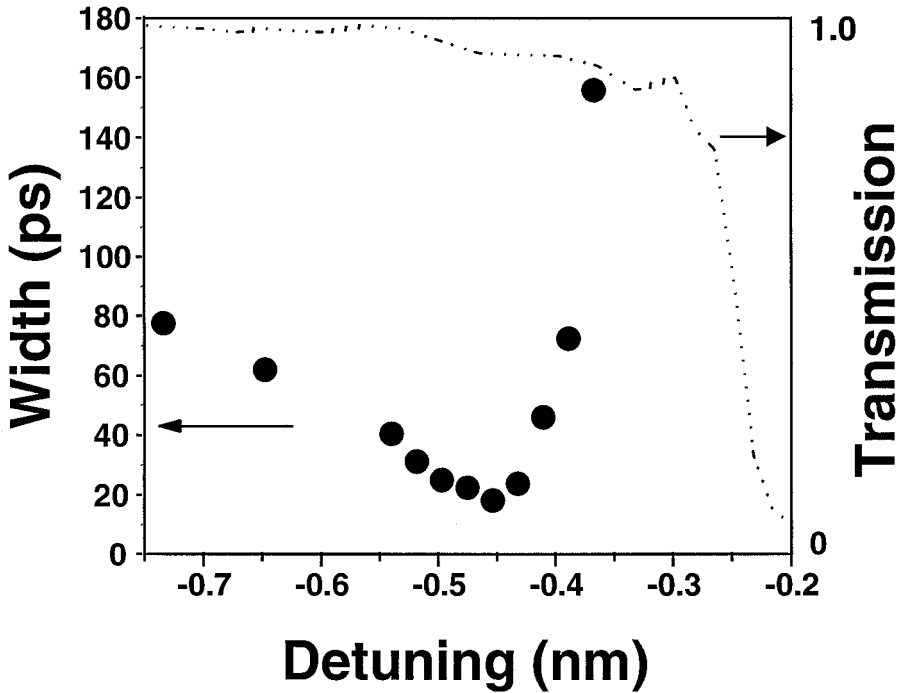


Figure 8. Deconvolved pulsewidth of transmitted pulse as a function of wavelength detuning ($\Delta\lambda$). Transmission spectrum of apodized Bragg grating is superimposed.

- (1) increasing the grating strength and length, which can reduce cubic dispersion thus improving the FOM F ;
- (2) linearizing the chirp of the spectrally broadened pulse by the effects of positive dispersion [5, 19], which is discussed in the next section;
- (3) using a saturable absorber or intensity discriminator [39, 40], which can attenuate the wings of the pulse.

The spectral broadening occurs because of SPM in the rod of a modelocked/Q-switched YLF laser. It is emphasized that this effect is known to occur in a wide class of high power modelocked/Q-switched lasers [37]. A transmission grating could be a valuable component for compressing chirped pulses generated by high power lasers or for chirped pulses generated by gain-switched semiconductor lasers [41]. For the compression of high power pulses, nonlinearities in the grating can reduce the compression. In a scheme recently proposed by Galvanauskas et al. [42], a chirped Bragg grating was imprinted in bulk glass allowing for the compression of high power pulses.

Pulse Compression Using Fiber Gratings as Highly Dispersive Nonlinear Elements

Principle

As was discussed in the first section, compressing a transform-limited pulse requires spectral broadening that can be achieved by using SPM. However, pure SPM (for nonlinear phase

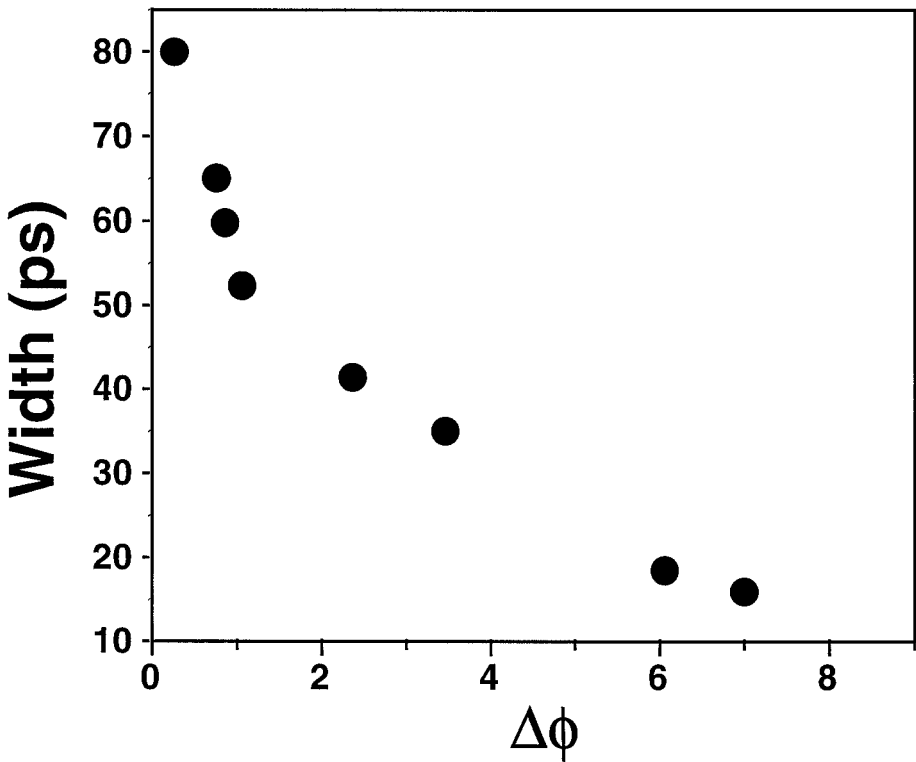


Figure 9. Deconvolved pulsewidth of transmitted pulse as a function of nonlinear phase shift ($\Delta\phi$).

shifts of a few π) leads to nulls in the pulse spectrum and results in a distorted compressed pulse in the time domain (c.f. Figures 5 and 7), which cannot be removed by a *linear* system (i.e., one containing only GVD). For this reason both SPM and positive GVD are required in order to produce compressed pulses close to the transform limit.

In this section, it is shown by using both the strong positive GVD and the SPM of a grating, square pulses with linear chirp across them can be produced. Once the linearly chirped square pulse emerges from the grating the chirp can be compensated by a linear element with negative GVD—either a diffraction grating pair or prism pair—resulting in a clean approximately transform-limited pulse. If the nonlinearity is small enough or the peak power is low enough (such that the grating length $L_g \ll L_{NL}$), then a second fiber grating may be used since it has opposite sign GVD on the two sides of the stop band. Figure 10 illustrates the principle of the Tomlinson Bragg grating compressor, which could be an all-fiber device if the second section consists of either a transmissive Bragg grating or a chirped grating operating in reflection [43].

Design of Pulse Compressor

In this section the achievable compression factors and required grating parameters are estimated. The pulse compression technique is governed by two important parameters [4]:

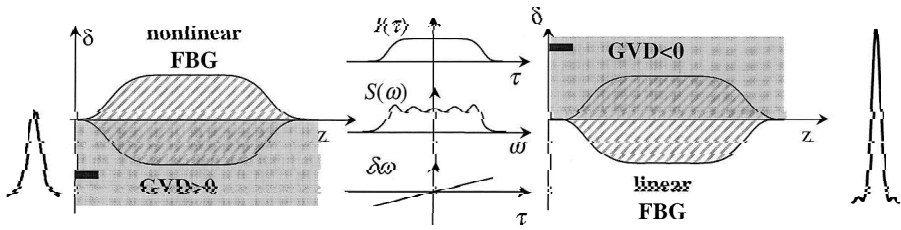


Figure 10. A schematic drawing of the Tomlinson Bragg grating compressor. The first section generates bandwidth and linearizes chirp and the second section compensates this chirp. Ideally, the result is an almost transform limited compressed pulse.

$$N = \sqrt{\frac{L_D}{L_{NL}}}$$

$$z_{opt} \approx \sqrt{6L_D L_{NL}} \quad \text{for } N \gg 1, \tag{25}$$

where z_{opt} is the length of fiber required for optimum compression. If $z < z_{opt}$ the chirp is not linearized yet, and if $z > z_{opt}$ the GVD-induced pulse broadening and corresponding reduction in peak intensity leads to SPM losing its effectiveness. In this case, the compression factor, $C = \tau_0/\tau_c$ (where τ_0 is the initial pulse-width and τ_c is the compressed pulse-width), is related to N through

$$C \approx N/1.6. \tag{26}$$

Since the compression factor scales with N it is clear that for maximum compression, one would like to operate at the lower limit of the nonlinear length and at the same time maximize the dispersion length. However, by increasing the dispersion length, the optimum length will increase and one is limited by the grating lengths that are technologically feasible. A good measure would be the ratio of the optimum length as defined in eq. (25) and the grating length L_g

$$q \cong \frac{z_{opt}}{L_g} \approx \left(6 \left(\frac{L_D}{L_g} \right) \left(\frac{L_{NL}}{L_g} \right) \right)^{1/2}. \tag{27}$$

Ideally one would like $q = 1$ which, for a given L_{NL} , will put an upper limit on the dispersion length.

The general design criteria are limited by the peak intensity and the higher order dispersion of the grating. High peak intensity is detrimental because it can lead to:

- 1) SRS,
- 2) shifting of the Bragg resonance,
- 3) truncation of the pulse spectrum by the photonic band gap.

Higher order dispersion leads to pulse distortion as shown earlier and ultimately limits the bandwidth over which efficient pulse compression can be achieved. The limits imposed by these different effects on the design of the fiber grating is examined.

The threshold for CW SRS dictates a worst case upper limit on the peak power as follows [4]:

$$P < \frac{16A_{eff}}{Lg_R}, \quad (28)$$

where g_R is the Raman gain coefficient at the wavelength of operation. This threshold leads to a lower limit of L_{NL}

$$L_{NL} > \frac{g_R \lambda}{32\pi n_2} L. \quad (29)$$

When pulses are considered, the actual peak power may be higher than eq. (28) suggests, since there is a walk-off between the pump and the Stokes pulse because of the strong GVD in the grating [4]. For short pulses, the Stokes pulse stops growing after three walk-off distances, [4] defined as $L_w = \tau_0 / (|v_p - v_s|)$, where v_p and v_s are the pump and Stokes pulse group velocities, respectively. To get an estimate for these effects one gives the following example. For a 60 ps (FWHM) pump pulse with a center wavelength of 1.06 μm and a Stokes pulse with a center wavelength of 1.12 μm propagating in a fiber grating with a coupling coefficient $\kappa = 32.4 \text{ cm}^{-1}$ and a detuning parameter for the pump pulse $\delta = -80 \text{ cm}^{-1}$, the walk-off distance is about 7.5 cm, for an optimum grating length of 63.5 cm. For this example, the Raman threshold is about 100 kW, which is much higher than the peak powers used in typical fiber grating experiments. Obviously, one of the advantages of using fiber gratings instead of optical fiber itself is that Raman gain does not impose as serious limitations on the peak power.

The next limit is specific to fiber gratings and is associated with an intensity-dependent shift in the Bragg resonance which leads to intensity-dependent dispersion. It can be shown that, for $\kappa \ll \delta_0$, $L_{NL}\delta_0 \gg 1$ is required to minimize this effect, which means increasing the detuning or decreasing the intensity of the pulse. Here δ_0 is the low intensity detuning parameter [19].

The last limitation imposed by the peak intensity is caused by SPM-induced spectral broadening of the input pulse spectrum. This broadening will be approximately C , since this is the intended purpose of the compressor. One now has to ensure that this spectrum does not overlap with the reflection spectrum of the grating, since this would cause truncation of the spectrum. The input bandwidth (at 1/e-level) of a transform-limited Gaussian pulse of width τ_0 is given by $\Delta\nu = 1/(2\pi\tau_0)$ and the output spectral bandwidth is approximately $(C/2\pi\tau_0)$. This spectral bandwidth must be smaller than the spectral distance from the band edge ($|\delta| = \kappa$)

$$|\delta| - \kappa > \frac{1}{V} \frac{C}{\sigma_0}. \quad (30)$$

Finally, one considers a purely linear property of the grating, namely, the higher order dispersion. As shown earlier, this limitation comes from the FOM— F . Using eq. (16) and given a grating strength, we get a lower limit on the detuning parameter,

$$|\delta| > \frac{3F}{2\sigma_0 V} + \left(\left(\frac{3F}{2\sigma_0 V} \right)^2 + \kappa^2 \right)^{1/2}, \quad (31)$$

which in turn will put an upper limit on the GVD. If we define δ_c as the limiting value above, the upper limit on the GVD can be written as

$$\beta_2 < \left(\frac{1}{V} \right)^{1/2} \left(\frac{\sigma_0}{3\delta_c F} \right)^{3/2} \kappa^2. \quad (32)$$

We can now place a lower limit on the dispersion length by using its definition (see eq. (1))

$$L_D > \sqrt{V} (3\delta_c F)^{3/2} \frac{\sqrt{\sigma_0}}{\kappa^2}. \quad (33)$$

As we mentioned, by increasing L_D , the optimum grating length will increase.

To demonstrate the effect of third-order dispersion on compression one adds a small amount of cubic dispersion to an ideal compressor, which contains only GVD and SPM and simulates using the NLSE with a 70 ps transform-limited Gaussian input pulse. This approach corresponds to the NLSE description of a Bragg grating (see eq. (17)) with an additional term corresponding to third-order dispersion. Figure 11 shows the results of this simulation for three *initial* values of the F parameter introduced earlier. $F = \infty$ represents the ideal case of no cubic dispersion and $F = 10$ and 20 are also shown. As a point of reference: for standard fiber with the same input pulse, $F = 10^4$. As can be seen, third-order dispersion introduces some pulse asymmetry as well as some structure on the leading edge, which will cause some trailing energy on the compressed pulse. A reasonable F value, in this example, is therefore >20 . It is noted that since $F \sim \tau(z)$, where $\tau(z)$ is the decreasing pulse width, F decreases along the length of the grating.

Numerical Example

One now looks at the parameters required for pulse compression of a 60 ps Gaussian pulse with a center wavelength of 1.06 μm . The design parameters for a grating will be outlined, which will enable a compression of $C \approx 5$. The corresponding nonlinear length for an effective mode area of 50 μm^2 is $L_{NL} = 3.2$ cm, which may be used as a lower limit. To get a compression factor of 5, one needs to choose $L_D = 207.4$ cm with a corresponding GVD of 6.3 ps^2/cm and an optimum length of 63.5 cm. By choosing the detuning $\delta = -80$ cm^{-1} and the grating strength $\kappa = 32.4$ cm^{-1} , one gets an F parameter of 12 for the initial pulse width $\tau_0 =$

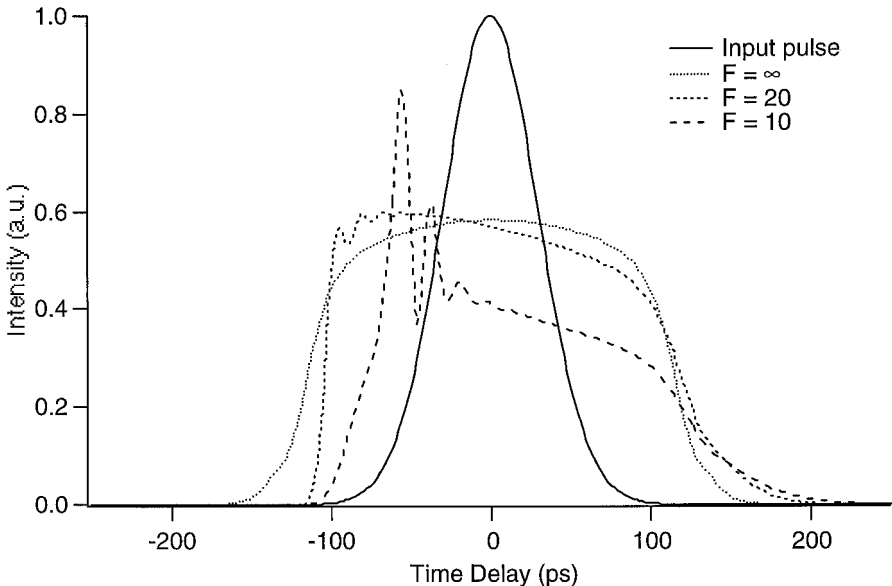
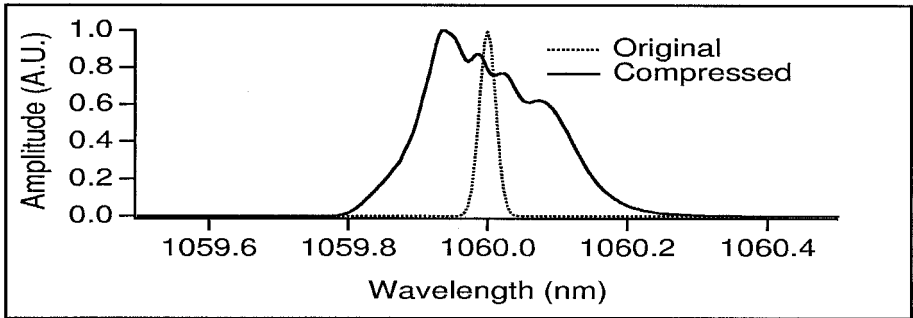


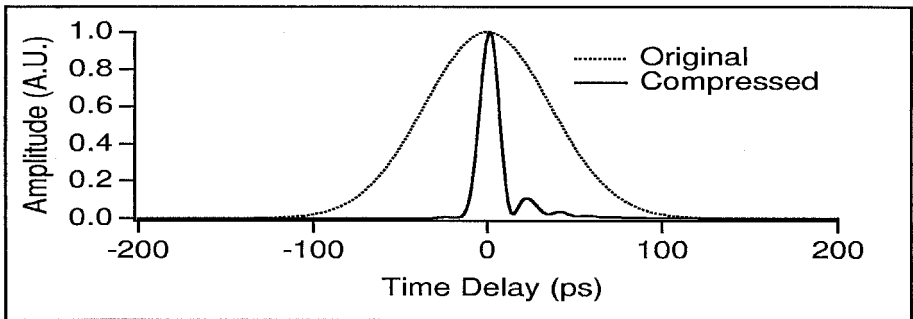
Figure 11. The effect of cubic dispersion on the compressor performance. F is a measure of the relative magnitude of quadratic and cubic dispersion (see text). This simulation assumes a 70 ps Gaussian pulse of 170 GW/cm^2 peak intensity propagating in a 10 cm homogeneous medium with $\beta_2 = 50$ ps^2/cm and $\beta_3 = 0, 175$ and 350 ps^3/cm for $F = \infty, 20$ and 10 , respectively.

36 ps, and $F = 2.4$ for the output pulse assuming the compression factor $C \approx 5$. It can be shown that a shorter grating of 20 cm will degrade the compression factor by less than 10% [19].

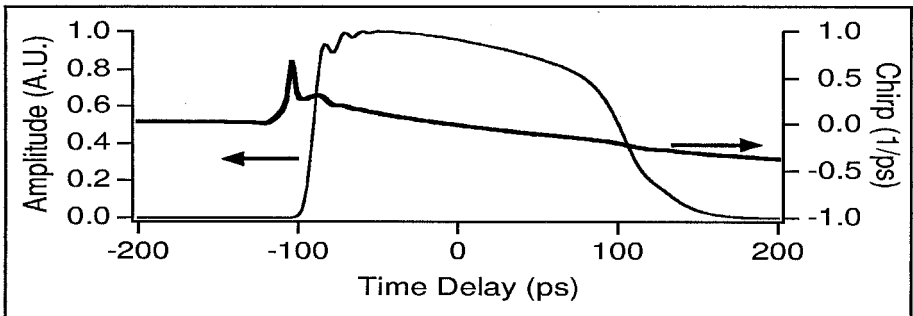
Using these parameters the propagation by two different techniques was simulated numerically: 1) a full numerical solution of the NLCME for the apodized grating, and 2) a split-step Fourier method of the NLSE (eq. 17), including both β_2 and β_3 . In both cases, one looks at the output pulse before the compensating section. In Figure 12a and 12b the input and



(a)



(b)



(c)

Figure 12. (a) Input 60 ps transform limited Gaussian pulse of 20 GW/cm² peak intensity and the final compressed pulse. (b) The corresponding spectra. (c) The pulse and its chirp after propagating through 63.5 cm of a homogeneous medium with $\beta_2 = 6.3$ ps²/cm and $\beta_3 = 18.9$ ps³/cm.

output pulse are shown, respectively, in the time and frequency domain. And in Figure 12c the pulse and the chirp are shown across the pulse just before the compensation section. As can be seen, the compressed pulse has some residual trailing energy in the time-domain and slightly asymmetric spectrum (both consequences of the small third-order dispersion), but it is still of reasonably high quality. Figure 13 compares the results of the two different simulation methods using the same parameters but with a grating length of 20 cm. Figure 13a shows the intensity profile of the pulse before the dispersion compensating section and 13b shows the resulting compressed pulse at the output of the system with a compression factor of 4.6 in good agreement with the analytical model.

Discussion

In this section, a compression scheme was considered that uses strong positive GVD achievable in the passband of fiber gratings for frequencies below the photonic bandgap. The scheme is superior to that described in a previous section, as it can result in clean optical pulses. However, it still requires a two-section device. In the next two sections pulse compression schemes are described that utilize only a single grating.

Analysis of the limitations placed on this system have been presented primarily by higher-order dispersion terms and high peak intensities. This analysis shows that the limitations imposed by SRS are not as severe in this scheme because of the short walk-off distance for pump and Stokes pulses. Numerical simulations show the performance predicted by analysis, as well as the close agreement between the results of the full NLCME and the NLSE.

Bragg Soliton-Effect Compression Using Nonlinear Bragg Gratings

Fiber-based soliton-effect compressors have been used to obtain very high compression factors [44]. However, like all other fiber-based compressors, they require a long length of fiber. By using a Bragg grating compressor one can reduce the length of the device from hundreds of meters to a few centimeters. In addition, as the dispersion is frequency-dependent, one can easily control the compression ratio by varying the parameters of the grating, e.g., by application of strain or temperature. In this section, a nonlinear pulse compression scheme is considered based on the *self*-compression of a N -soliton pulse in a single apodized Bragg grating. The principle of the Bragg soliton-effect compressor is illustrated in Figure 14; a single apodized Bragg grating is used and the pulse is detuned to frequencies below the photonic bandgap.

Here, the recent experiments are briefly reviewed studying nonlinear pulse and self-compression [29]. In this experiment 80 ps (FWHM) approximately transform-limited pulses generated by a modelocked/Q-switched YLF laser were coupled into a 7.5 cm long apodized fiber Bragg grating [29]. The bandwidth of the apodized grating was approximately 0.17 nm, corresponding to a strength of $\kappa = 7 \text{ cm}^{-1}$. Figure 15 shows an example of these results when the peak intensity of the pulses incident upon the grating was approximately 13 GW/cm^2 . In particular, Figure 15a shows the transmitted intensity versus time for different values of detuning. By varying the strain on the grating, one can change the detuning of the input pulse, and thus tune to different points on the dispersion curve. As mentioned above, one can thus, in effect, *tune* the dispersion length and therefore, N . Note from Figure 15 that far from the photonic band gap edge, where the grating-induced GVD is negligible, the pulse is unaffected and propagates through the grating at the speed of light. Closer to the edge of the photonic band gap, the pulse is substantially compressed; below it is shown that this can be understood in terms of soliton-effect compression. Note that the compressed pulse is slightly asymmetric

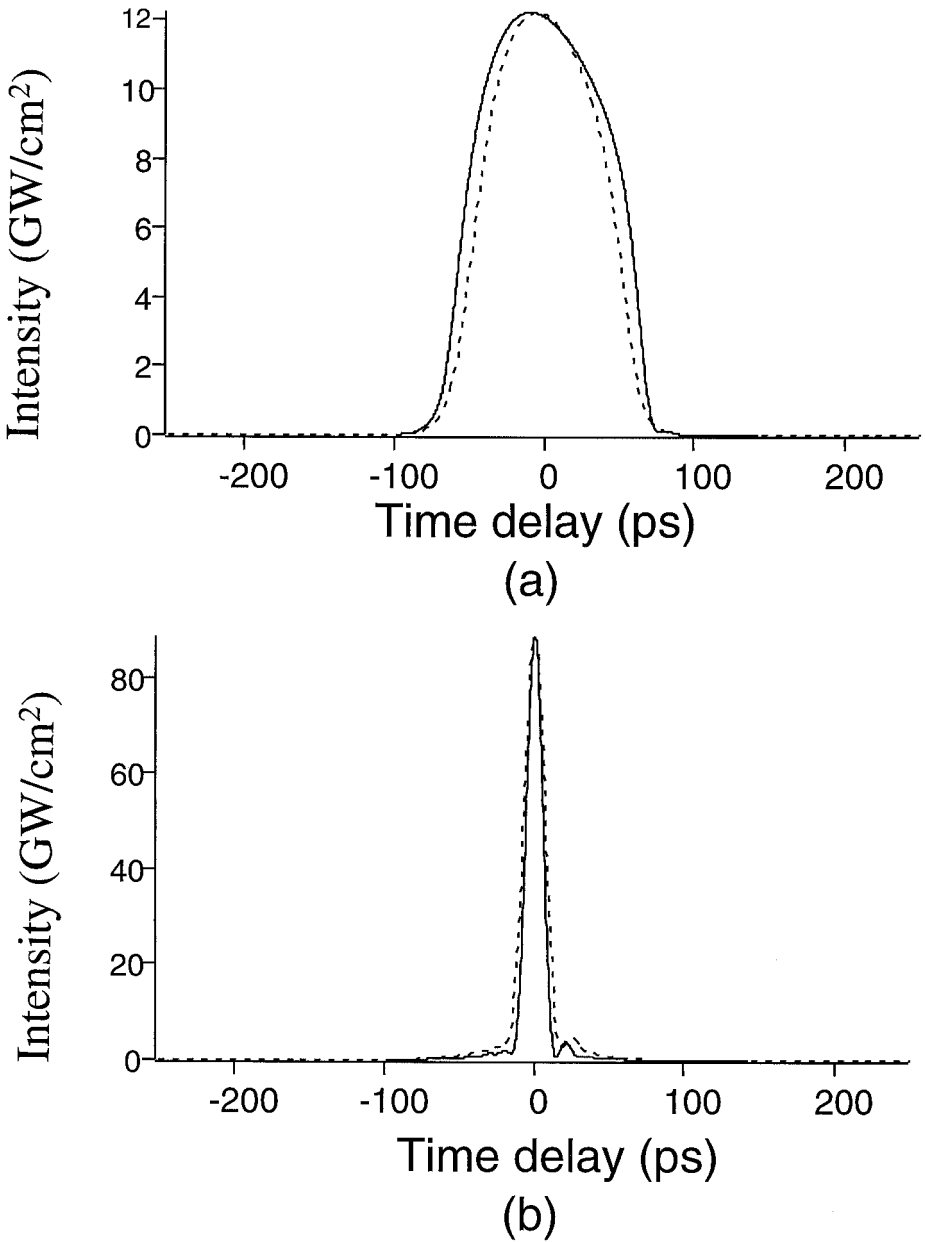


Figure 13. Comparison of simulation results using the split step Fourier method for the NLSE (dashed line) and the full NLCME for gratings (solid line). For (a), the pulse intensity profile before and for (b), after the dispersion compensating section.

and there is a small pedestal. In addition to this compression, the transmitted pulse is substantially delayed in time [45]. This retardation is simply caused by the reduced group velocity of the pulse propagating through the grating.

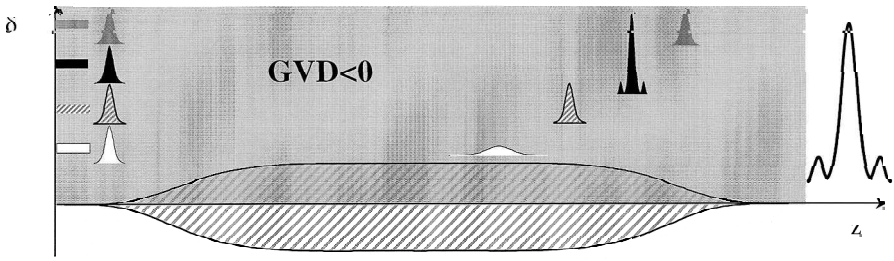


Figure 14. Schematic of Bragg soliton-effect compressor. For $N < 0.5$, the transmitted pulse is broadened due to the strong GVD of the grating and for $N \geq 2$, the pulse undergoes a periodic evolution associated with higher order solitons.

Figure 15b shows the FWHM of the transmitted pulse, versus detuning, for three different cases represents:

- (1) the experimental plots (dots);
- (2) simulated using the NLCME (dashed line);
- (3) simulated using NLSE (dotted line).

The agreement between experimental results and simulations of both NLCME and NLSE confirms that this experimental geometry can be well described by the NLSE. Therefore, one can apply the results obtained for NLSE to describe (at least qualitatively) the propagation of higher-order solitons in Bragg gratings, though no rigorous theory based on full NLCME for higher-order Bragg solitons has been developed to date.

Standard NLSE theory for solitons predicts that a $N = 1$ soliton maintains its shape and spectrum as it propagates through a nonlinear dispersive medium [4]. Besides the fundamental soliton, the NLSE generally has higher-order soliton solutions. At input powers corresponding to integer values of N , the soliton restores its shape and spectrum periodically at the characteristic length scale $z_0 = (\pi/2)L_D$ [39, 44]. In general, higher-order solitons evolve through many different stages including compression and various splittings. However, any $N \geq 2$ soliton always go through an initial compression at the beginning of each period. A simple estimation of the maximum compression ratio can be obtained from an approximate relation between the compression factor and an initial pulse amplitude (N)

$$C \approx 4.6(N - 1). \quad (34)$$

This relation is accurate to within 10% for $2 \leq N < 15$ [46]. For integer values of N , the inverse scattering method can be used to find the optimum compression factor and the optimum length of the compressor [4]. Note that for noninteger values of N , the pulse shape and spectrum at $z = z_0$ are different from those at $z = 0$.

Temporal and spectral evolution of higher-order solitons can be understood by considering the mutual interplay between SPM and GVD. Self-phase modulation generates a positive frequency chirp and extra bandwidth, while negative GVD compensates for the SPM-induced chirp and compresses the pulse. As the SPM-induced chirp is only linear near the central frequency of the pulse, only the central portion of the pulse is compressed. Therefore, the

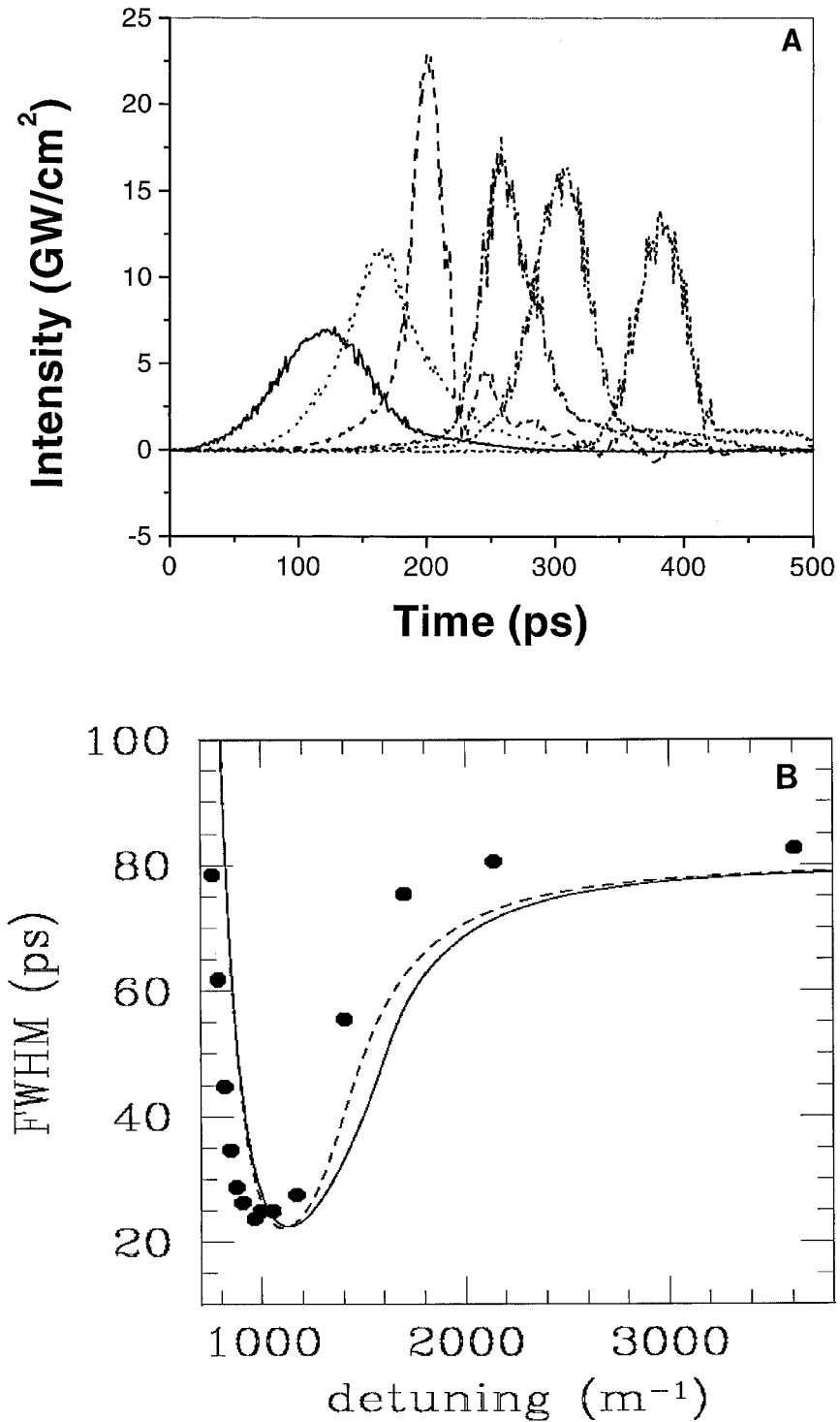


Figure 15. Experimental results of nonlinear pulse propagation in apodized fiber Bragg grating. (a) Intensity versus time after propagation through the grating at a peak intensity of 13 GW/cm², for several different values of the detuning and (b) width of transmitted pulse; (i) experimental, (ii) calculated using NLCME, and (iii) calculated using NLSE.

compressed pulse is accompanied by a significant pedestal. Another limitation is that modulation instability leads to pulse decay before the optimum self-compression is achieved.

Soliton-compression effect is illustrated using as an example propagation of a $N = 2$ soliton in an apodized fiber grating. It will be shown that the compressed pulse shown by the dashed line in Figure 15a approximately corresponds to a $N = 2$ soliton for the set of parameters in the experiment. The optimum compression length in this case occurs at $z = z_0/2$ and the maximum compression factor is 4 [47]. In order to observe a compressed pulse at the output for our grating, one should choose the parameters so that $z_0/2 \approx L$. Note that z_0 does not depend on N . Requiring $z_0/2 = L = 7.5$ cm, from eq. (22), one obtains $\beta_2 = -215$ ps²/cm, which corresponds to the detuning $\delta \approx 10.85$ cm⁻¹. Then, using eq. (20), it is estimated that the input intensity necessary to launch a $N = 1$ soliton is $I_{out} = 3.2$ GW/cm². The two-soliton threshold is a factor of $(1.5)^2$ larger than this, i.e., roughly 7.2 GW/cm² and the intensity of $N = 2$ soliton is $4I_{out} \approx 13$ GW/cm². Figures 15a and b show that maximum compression occurs at detunings ~ 11 cm⁻¹ and the FWHM of the compressed pulse is ~ 20 ps, which corresponds to a compression factor of 4, in good agreement with the theoretical predictions.

Bragg soliton effect compression is a simple method for achieving picosecond pulse compression that utilizes only a single apodized Bragg grating. Because the dispersion is frequency dependent, the compression ratio can easily be controlled simply by varying the parameters of the grating, e.g., by application of strain or temperature. It has the disadvantage that the compressed pulse is accompanied by a pedestal. In the next section, a compression scheme is presented that utilizes only one grating and can produce clean pulses.

Adiabatic Bragg Soliton Compression

Principle

A novel technique for optical pulse compression makes use of “soliton robustness” in optical fibers in which the dispersion decreases along the direction of propagation in the fiber [48, 49]. As discussed in the first section, the principle of *adiabatic soliton compression* is that if the dispersion varies slowly enough (i.e., the variations are *adiabatic*), a soliton self-adjusts to maintain the balance between dispersion and nonlinearity. This principle may be used to manipulate and adjust a soliton shape and “trajectory” resulting in a reduction in the pulse width—hence the term adiabatic compression.

As with most pulse-shaping techniques using optical fiber, the low fiber dispersion leads to large dispersion lengths and long fiber lengths for picosecond pulses. A larger dispersion would lead to a decrease in L_D and a corresponding reduction in the size of the fiber-based device. As discussed earlier, periodic media (including fiber Bragg gratings [FBGs] and photonic band gap structures) have an associated large dispersion in the spectral region close to the reflection band of the medium. Furthermore, dispersion “engineering” is simpler since different gratings can be easily cascaded or chirped making the effective dispersion much easier to handle, compared to splicing many different fibers or making a fiber with an axially tapered core. FBGs have a number of further advantages. By straining or heating the grating parameters such as the center wavelength, the grating chirp and thus the dispersion profile may be adjusted [50–52].

In this section, adiabatic soliton compression is discussed using a nonuniform Bragg grating. The principle is illustrated in Figure 16, which shows a dispersion-decreasing structure (i.e., a nonuniform FBG) being used to achieve adiabatic soliton compression in typical length FBGs. We extend the NLSE description outlined in a previous section to allow for axial variations in the GVD and the nonlinearity. This technique allows for describing pulse evolution and compression in a structure possessing strong position-dependent dispersion, such as a nonuniform Bragg grating. This model is used to derive design equations for compressing picosecond pulses and, in particular, in considering the adiabatic condition.

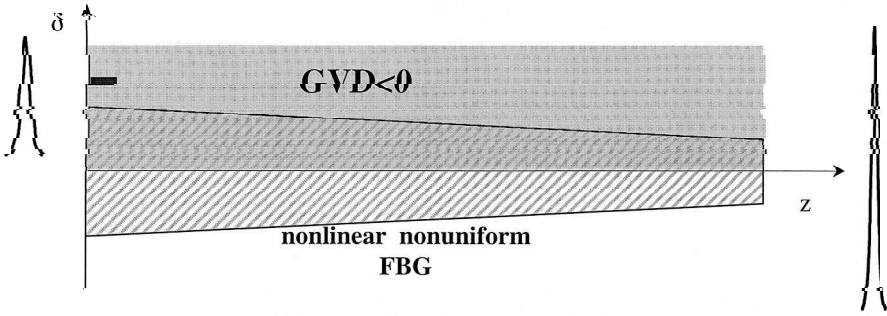


Figure 16. Schematic illustration of an adiabatic Bragg soliton compressor based on an apodized FBG with an index modulation that decrease linearly along the grating. The shaded region shows the top band region as a function of position along the fiber. The detuning of the pulse center frequency relative to the Bragg frequency is constant in this example.

Numerical simulations using the NLCME, which describe propagation in such structures, confirm the predictions made by this model.

Nonlinear Propagation in Nonuniform Bragg Gratings

In this section a simple model for adiabatic soliton compression in a nonuniform FBG is established using the NLSE with z -dependent coefficients. Once again, it is emphasized that this description is only an approximation valid under certain circumstances. A more complete description based on a modified NLSE has been recently developed [53]; however, it is beyond the scope of this paper. Following [8] the NLSE is written

$$i \frac{\partial A}{\partial z} - \frac{\beta_2(z)}{2} \frac{\partial^2 A}{\partial t^2} + \Gamma(z) |A|^2 A = 0. \quad (35)$$

This equation allows for varying quadratic dispersion (second term), varying effective area, and hence effective nonlinearity (third term). Using eq. (20), the following condition is obtained for maintaining $N = 1$ soliton in a nonuniform Bragg grating

$$E_S = \frac{\pi n_2}{A_{\text{eff}} \lambda} \frac{\alpha(z)}{|\beta_2^{\text{eff}}(z)|} = 1, \quad (36)$$

where β_2^{eff} is an *effective* GVD defined to include the frequency dependence of both β_2 eq. (14) and Γ eq. (18)

$$\beta_2^{\text{eff}}(z) = - \frac{2\kappa^2(z)\delta}{V^2(2\delta^2 + \kappa^2(z))(\delta^2 - \kappa^2(z))}. \quad (37)$$

In the following, normalized quantities are used to conform to the notation introduced in [8]. By using the transformations

$$\begin{aligned} \xi &= \frac{1}{\alpha_0^2} \int_0^z \beta_2(z') dz' \\ \Psi &= A(z) \sqrt{\Gamma(z)/\beta_2(z)}, \end{aligned} \quad (38)$$

where τ_0 is the input pulse width and β_2 is assumed negative, one can now write eq. (35) as

$$i \frac{\partial \Psi(\xi, \sigma)}{\partial \xi} + \frac{1}{2} \frac{\partial^2 \Psi(\xi, \sigma)}{d\sigma^2} + |\Psi(\xi, \sigma)|^2 \Psi(\xi, \sigma) - i\alpha(\xi)\Psi(\xi, \sigma) = 0, \quad (39)$$

for decreasing GVD and nonlinearity $\alpha(\xi)$ representing an effective gain. In this case, where only the dispersion and nonlinearity vary and there is no loss or gain in the fiber, this gain term is given by

$$\alpha(\xi) = \frac{-\partial\beta/\partial\xi}{2\beta} + \frac{\partial\Gamma/\partial\xi}{2\Gamma} \equiv -\frac{1}{2\beta_2^{eff}} \frac{\partial\beta_2^{eff}}{\partial\xi}. \quad (40)$$

As in [8] the total integrated gain is also defined

$$W_{eff}(\xi) = \exp\left[2 \int_0^\xi \alpha(\xi') d\xi'\right], \quad (41)$$

which in this case reduces to

$$W_{eff}(z) = \frac{\beta_2(0) \Gamma(z)}{\beta_2(z) \Gamma(0)} = \frac{\beta_2^{eff}(0)}{\beta_2^{eff}(z)}. \quad (42)$$

This simplification means that the total effective gain depends only on the value of the effective dispersion at the endpoints. Furthermore, since $|\beta_2^{eff}(z)|/\tau(z)$ must remain constant, W_{eff} also gives the total pulse compression ratio making it one of the key parameters in this scheme. Note that the compression factor depends only on the ‘‘endpoints’’ and is independent of the exact functional form of the dispersion, as long as the process is *adiabatic* along the entire propagation length. The change in dispersion has to be gradual enough such that the fundamental soliton is maintained and energy lost to continuum radiation is negligible.

For the compression process to be adiabatic, it is required that the gain coefficient g is small enough ($\alpha L_D \ll 1$), so that little amplification occurs over L_D . If $\alpha(\xi)$ varies slowly with ξ , it can be averaged over the grating length. From eq. (41) $W_{eff} = e^{2\alpha L}$, which implies the adiabatic condition

$$\frac{L_D}{2L} \ln(W_{eff}(L)) \ll 1. \quad (43)$$

From this expression it is concluded that satisfying the adiabatic condition requires one or more of the following: large lengths, short input pulses, large input dispersion. The pulse width at the grating output can now be written as

$$\alpha(L) = \frac{\sigma_0}{W_{eff}(L)}, \quad (44)$$

where W_{eff} represents the compression factor.

These results may now be used for designing nonuniform FBGs adiabatic soliton compressors. As pointed out earlier, cubic dispersion needs to be considered, and in general, one will operate at a detuning where F is large, such that the above results are a good approximation. In the next section, the effects of cubic dispersion in our numerical simulations are investigated and one will restrict oneself to the case of varying index modification only while keeping the detuning constant (see Figure 16). The simplest case is a linearly decreasing coupling coefficient $\kappa(z)$, and since δ is fixed, a linear function result given by

$$\kappa(z) = \kappa(0) + (\kappa(L) - \kappa(0)) \frac{z}{L}, \quad (45)$$

where L is the FBG length. The corresponding compression factor according to eq. (42) is

$$W_{\text{eff}}(L) = \frac{\kappa^2(0) (\delta^2 - \kappa^2(L)) (2\delta^2 + \kappa^2(L))}{\kappa^2(L) (\delta^2 - \kappa^2(0)) (2\delta^2 + \kappa^2(0))}. \quad (46)$$

Note again that this result for the compression factor does not depend on the functional form of $\kappa(z)$ and will be the same for any function $\kappa(z)$ with the same initial and final points, as long as the adiabatic condition is satisfied, as was explained earlier. The second relevant parameter is the integrated dispersion. Using eq. (38) and performing the integration one finds [20]

$$\xi = f(\kappa, \delta) \frac{L}{\sigma_0^2}. \quad (47)$$

The integrated dispersion, ξ , is proportional to L/σ_0^2 and the proportionality factor $f(\kappa, \delta)$ [20]. The adiabatic condition, as described in eq. (43), however, implies a lower limit on L/σ_0^2 .

The constraints on ξ and L/σ_0^2 mean that the above prefactor f has to be made suitably small. This can be done by choosing κ and δ correctly.

This section is concluded with the following observations. First, the compression factor and adiabatic condition are functions of $\kappa(0)$ and $\kappa(L)$ only. Second, the scaling parameter L/σ_0^2 depends additionally on the difference $\kappa(0) - \kappa(L)$ [20] and determines the relation between the grating length and input pulse width. Since FBGs are currently limited to lengths on the order of 1 m, there is an upper limit on the input pulse width.

Numerical Examples

Next a numerical example is presented with a compression factor of ~ 3 and higher-order dispersion effects are minimized. The split step Fourier scheme is first used, where at each step one inserts the value of the quadratic and cubic dispersion at that position. Results are compared with the numerical solution of the NLCMEs. In this example a linear variation is used in the refractive index modulation. The Bragg wavelength in this example is set to 1.550 μm . The initial and final coupling constant is $\kappa(0) = 81.07 \text{ cm}^{-1}$ and $\kappa(L) = 48.64 \text{ cm}^{-1}$, respectively. The detuning parameter is chosen to be twice the initial coupling constant: $\delta = 2\kappa(0) = 162.14 \text{ cm}^{-1}$. The GVD at the endpoints may now be calculated and give $\beta_2(0) = -5.546 \text{ ps}^2/\text{cm}$ and $\beta_2(L) = -1.494 \text{ ps}^2/\text{cm}$. Similarly, one can calculate the cubic dispersion at the endpoints, where $\beta_3(0) = 6.613 \text{ ps}^3/\text{cm}$ and $\beta_3(L) = 1.468 \text{ ps}^3/\text{cm}$. The grating is assumed to be apodized and 1 m long ($L = 100 \text{ cm}$). For the NLCME simulation, 2.5 mm long apodized regions were included at the ends of the grating, adding a negligible non-linear phase shift of less than 0.1 radians. For the input field one uses a fundamental soliton with a field distribution given by $E = A_0 \text{sech}(t/\tau_0)$ with $\tau_0 = 10 \text{ ps}$. With a center wavelength of $\lambda = 1.546 \mu\text{m}$, which is detuned from the Bragg wavelength, one finds the required input intensity to be $I \sim 5.9 \text{ GW}/\text{cm}^2$. Assuming an effective mode area of $A_{\text{eff}} = 20 \mu\text{m}^2$, one calculates a corresponding input peak power of $P = 1.2 \text{ kW}$ peak power and an energy of 24 nJ, for a sech pulse.

From eq. (46) and the above values of the quadratic dispersion one expects a compression factor of ~ 3.1 . In this case $aL_D \sim 0.1$ and the adiabatic condition (see eq. (43)) is easily met. Finally, the F parameter at the input and output is ~ 8 and ~ 3 , respectively. Figure 17 shows the result of the NLSE simulation with and without the effects of cubic dispersion, and the inset shows the evolution of the pulse in the grating. As can be seen, the pulse evolution is smooth and there is no visible degradation caused by the cubic dispersion.

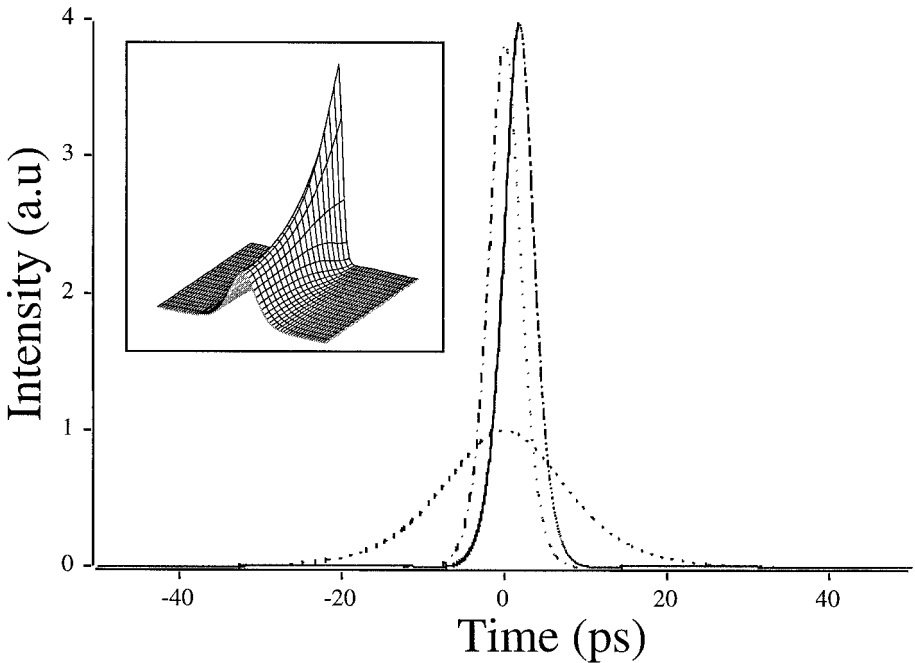


Figure 17. Simulation of adiabatic soliton compression in a 100 cm long grating with cubic dispersion (solid line) and without cubic dispersion (dash-dotted line). The input pulse (dashed line) is a fundamental soliton with pulse width of 17.6 ps. See text for other parameters. The inset shows the soliton evolution along the grating.

In the second simulation the same parameters are used to numerically solve the NLCME for this nonuniform grating. Figure 18 shows a comparison of the results from both simulations as well as the analytic result, which ignores the cubic dispersion. As can be seen, the compression is of high quality in all cases. In both simulations one finds a dip in the center of the spectrum, which does not seem to impact the quality of the compressed pulse in the time-domain, but indicates that the compressed pulse is not a perfect $N = 1$ soliton. This “imperfection” shows up in the time-domain as a very small pedestal (not visible on a linear scale) and may be caused by finite radiation coupled to the continuum.

High Repetition Rate Pulse-Train Source

Finally, a high-repetition-rate soliton source is presented based on adiabatic compression of a signal created by beating two CW lasers together and propagating this beat signal in a nonuniform fiber Bragg grating (see Figure 19 for a schematic representation). As the signal propagates through the grating, whose index modulation depth decreases along its length, it is reshaped into a train of solitons through adiabatic compression, as was discussed in the previous section [54]. The repetition rate of the output pulse train is given by the frequency separation between the spectral components creating the signal [54].

Although the simple analytical model developed in a previous section assumes that the input pulses are solitons, it predicts the width of compressed soliton-like pulses even if the input signal is sinusoidal and it also provides conditions for adiabatic compression.

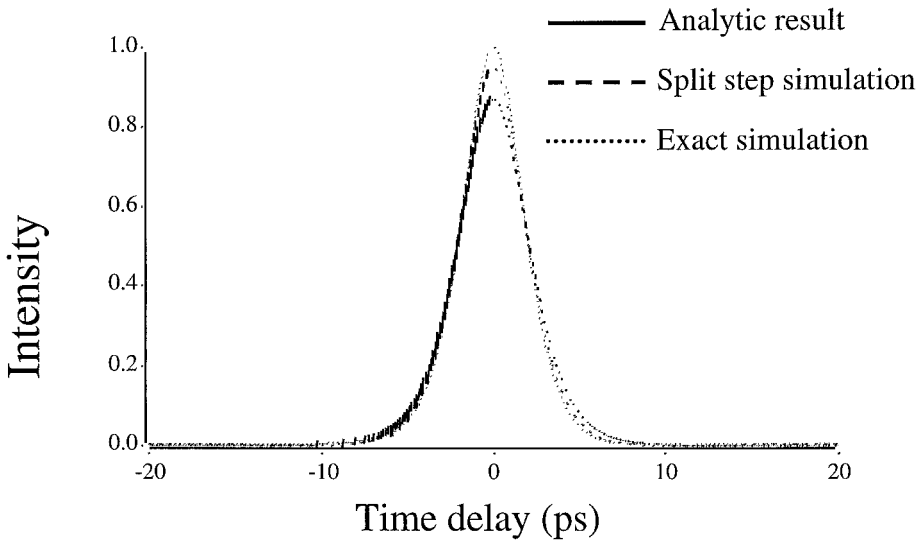


Figure 18. Comparison of analytic result (solid line) numerical simulation using the split step method (dashed line) and the numerical solution of the nonlinear coupled-mode equations (dotted line). In all cases, the launched intensity profile was $\text{sech}^2(t/10)$ with t in picoseconds. The peak intensity was 5.93 GW/cm^2 for the first two cases and 5.5 GW/cm^2 for the second case.

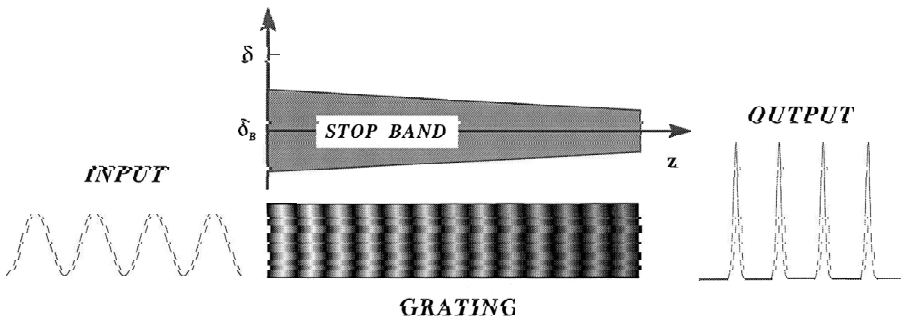


Figure 19. Generation of a high-repetition rate soliton train based on adiabatic Bragg soliton compression in a nonuniform Bragg grating.

The optical beat signal can be obtained from a laser operating simultaneously in two longitudinal modes, by using two distributed feedback semiconductor lasers, each operating in a single longitudinal mode; or by phase modulating a single CW laser and beating one pair of sidebands [55]. Coherent beating between the two modes generates a sinusoidally modulated optical signal such that

$$A(t, 0) = A_0 \sin(\pi t/T_S), \quad (48)$$

where $T_S = (\Delta\nu)^{-1}$ is the modulation period for a frequency spacing of $\Delta\nu$. A fiber grating is again considered whose coupling coefficient is linearly varying along the length of the grat-

ing and of the general form of eq. (45). Numerical simulations of NLCMEs are now performed. As an example, one considers propagation of a 40-GHz sinusoidal signal with $T_S = 25$ ps and $I_{out} = 7.04$ GW/cm² through a 70-cm-long apodized fiber grating. The κ profile is given by eq. (45) with $\kappa(0) = 80$ cm⁻¹, $\kappa(L) = 38.3$ cm⁻¹, $\delta = 160$ cm⁻¹ so that $W_{eff} = 5$. Since $\alpha L_D \approx 0.1$ for this choice of parameters, the adiabatic-compression condition is reasonably well satisfied. Figures 20 and 21 show pulse shapes and spectra, respectively, at the input (upper plot) and output (lower plot) ends of the grating. These results show that as the 12.5-ps sinusoidal waveform evolves, each half-cycle is compressed by a factor of about 4.8 to become 2.6 ps soliton-like pulses. This behavior is in good agreement with the prediction of our simple analytic theory [54]. Note that each pulse in the generated train contains a very small pedestal, which is not visible on a linear scale. The origin of the pedestal may be related to the fact that the compression is not perfectly adiabatic, resulting in an asymmetric spectrum as seen in Figure 21. The time-bandwidth product for each pulse in the train is found to be about 0.34 (FWHM) compared to 0.315 for a soliton, which means that the pulses are very close to transform-limited. Finally, note that in this example, the ratio between the soliton separation and soliton pulse width is 9.6. Since the pulses are widely separated, neighboring solitons practically do not interact with each other [56].

Discussion

To summarize this section, it has been shown that dispersion-decreasing FBGs allow for adiabatic soliton compression in very short sections of fiber, leading to a novel all-fiber compression device. Because the dispersion of the grating is easily tailored during the writing process, this device is highly versatile—it does not require specialty fiber and does not require the splicing together of many different fibers to achieve the desired dispersion profile. Also proposed has been a high-repetition-rate soliton-train source based on a dual-frequency signal being reshaped into a train of soliton-like pulses as it is compressed adiabatically during its propagation along the grating.

The main shortcoming of this compression scheme comes from the inherent high cubic dispersion, which ultimately limits the compression factor. Our simulations show that factors of 10 are easily achievable for ~ 20 ps (FWHM) pulses in ~ 150 cm gratings. Adiabatic compression of *Bragg solitons*, represented by the A&W solitary wave solutions [35], may overcome this limitation, since all orders of dispersion are implicitly balanced. At present, the manufacturable length of FBGs limits the input pulse width to a few tens of picoseconds; however, the rapidly improving FBG technology may extend this range considerably. The short compression length comes at a price of high-input intensity making these compressors very useful for high-power YAG-type systems. Using high- n_2 fiber, however, will scale the intensity down by at least two orders of magnitude making this compressor useful for many other laser systems.

Implicit in the NLSE description of adiabatic Bragg soliton compression is that the velocity of the evolving soliton was assumed to be invariant. Clearly, this cannot be the case in a grating in which the dispersion is varying with position. In these examples the soliton velocity accelerates by as much as 5%. In spite of this, the agreement was still very encouraging.

Discussion and Conclusion

A review of optical pulse compression and ultrashort pulse generation techniques has been presented that use nonlinear Bragg grating structures. The optical pulse compressors and generators that have been considered here are based on apodized fiber Bragg gratings that operate in *transmission*. By utilizing the strong GVD of Bragg gratings, as well as highly

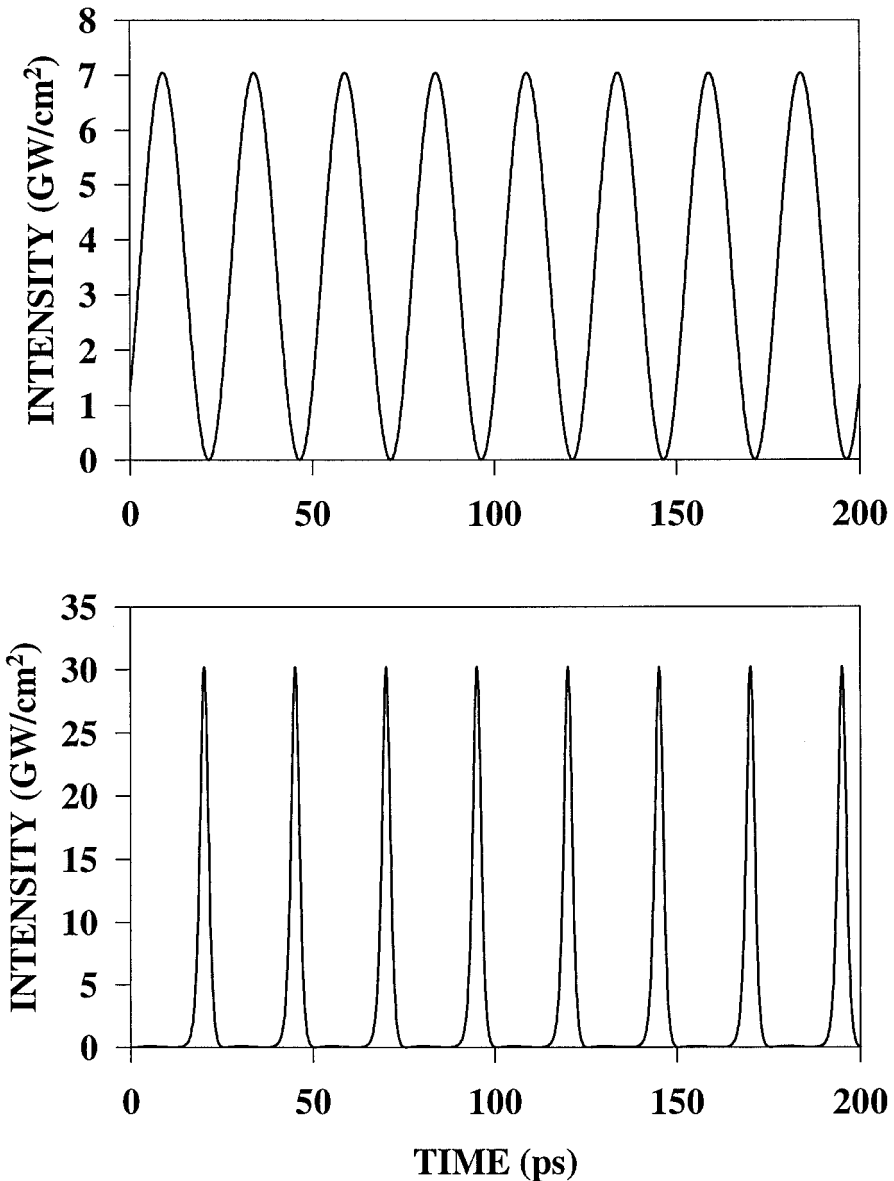


Figure 20. Input sinusoidal (upper plot) and soliton train generated at the grating output (lower plot).

nonlinear material such as chalcogenide, one can realize compact and efficient pulse compressors. Several different schemes were proposed and analyzed.

To summarize, the linear Bragg grating compressor relies only on the GVD of the grating to compress a pulse spectrally broadened and chirped only by SPM, in a separate component. The degree of compression in this case can be large, but the quality is not perfect because of the nonlinear chirp associated with SPM. Second, the Tomlinson Bragg grating compressor uses both the strong GVD and the Kerr nonlinearity of a fiber Bragg grating [19] to increase

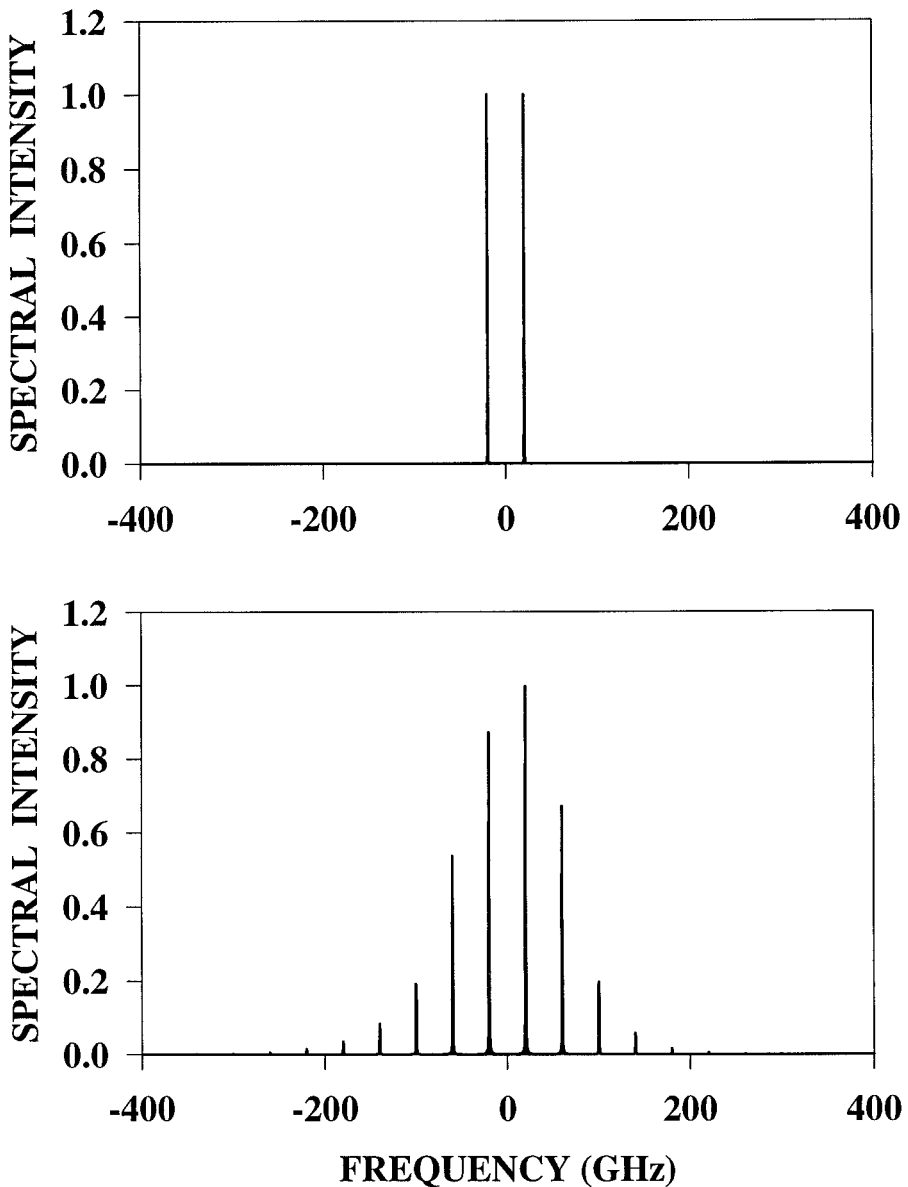


Figure 21. Input dual-frequency signal spectrum (upper plot) and output spectrum of the soliton train (lower plot).

the bandwidth and simultaneously linearize the chirp of the pulse. A second grating then acts as a chirp compensator (i.e., removes the mostly linear chirp). The pulse quality in this case is thus very good but the scheme requires two components. Third, Bragg soliton-effect compression was described, whereby a transform limited pulse undergoes an initial narrowing phase, through which all higher order solitons go before the initial soliton shape is restored after one soliton period fiber. This compression scheme has the advantage of it requiring

only one unchirped grating; however, the pulse quality is not high. Finally, a pulse compression scheme was described based on adiabatic soliton compression using a *nonuniform* grating in which the GVD decreased along the grating. This scheme has the advantage of requiring one component (i.e., one grating) and results in a clean transform limited pulse.

Finally, it should be noted that structures other than FBGs may be used for this compression scheme, such as deep-etched gratings with large Δn or other types of photonic crystals, where the structures' parameters may easily be controlled.

References

1. Diels, J.-C. and W. Rudolph. 1998. *Ultrashort laser pulse phenomena*, 1st ed. New York: Academic Press.
2. Ouellette, F., J. F. Cliche, and S. Gagnon. 1994. All-fiber devices for chromatic dispersion compensation based on chirped distributed resonant coupling. *Journal of Lightwave Technology* 12: 1728–1738.
3. Mollenauer, L. F., R. H. Stolen, and J. P. Gordon. 1980. Experimental observation of picosecond pulse narrowing and solitons in optical fibers. *Physics Review Letters* 45: 1095–1098.
4. Agrawal, G. P. 1989. *Nonlinear fiber optics*. San Diego: Academic Press.
5. Tomlinson, W. J., R. H. Stolen, and C. V. Shank. 1984. Compression of optical pulses by self-phase modulation in fibers. *Journal of Optical Society of America B*. 1: 139–143.
6. Fork, R. L., C. H. B. Cruz, P. C. Becker, and C. V. Shank. 1987. Compression of optical pulses to six femtoseconds by using cubic phase compensation. *Optics Letters* 12: 483–485.
7. Stolen, R. H., L. F. Mollenauer, and W. J. Tomlinson. 1983. Observation of pulse restoration at the soliton period in optical fibers. *Optical Letters* 8: 186–188.
8. Chernikov, S. V., and P. V. Mamyshev. 1991. Femtosecond soliton propagation in fibers with slowly decreasing dispersion. *Journal of Optical Society of America B*, 8: 1633–1641.
9. Kashyap, R. 1999. *Fiber Bragg gratings*, 1st ed. New York: Academic Press.
10. Russell, P. S. J. 1991. Bloch wave analysis of dispersion and pulse propagation in pure distributed feedback structures. *Journal of Modern Optics* 38: 1599–1619.
11. Eggleton, B. J., T. Stephens, P. A. Krug, G. Dhosi, Z. Brodzeli, and F. Ouellette. 1996. Dispersion compensation over 100 km at 10 Gbit/s using a fiber grating in transmission. *Electronics Letters* 32: 1610–1611.
12. Litchinitser, N. M., B. J. Eggleton, and D. B. Patterson. 1997. Fiber Bragg gratings for dispersion compensation in transmission: Theoretical model and design criteria for nearly ideal pulse compression. *Journal of Lightwave Technology* 15: 1303–1313.
13. Eggleton, B. J., R. E. Slusher, C. M. D. Sterke, P. A. Krug, and J. E. Sipe. 1996. Bragg grating solitons. *Physical Review Letters* 76: 1627–1630.
14. Asobe, M. 1997. Nonlinear optical properties of chalcogenide glass fibers and their application to all-optical switching. *Optical Fiber Technology* 3: 142–145.
15. Scalora, M., R. J. Flynn, S. B. Reinhardt, R. L. Fork, M. D. Tocci, M. J. Bloemer, C. M. Bowden, H. S. Ledbetter, J. M. Bendikson, J. P. Dowling, and R. P. Heavitt. 1996. Ultrashort pulse propagation at the photonic bandgap edge: large tunable delay with minimal pulse distortion. *Physics Review E*. 54: 1078–1082.
16. Conti, C., G. Assanto, and S. Trillo. 1998. Parametric gap solitons in quadratic media. *Optics Express* 3: 389–404.
17. Taverner, D., N. G. R. Broderick, D. J. Richardson, R. I. Laming, and M. Ibsen. 1998. Nonlinear self-switching and multiple-gap soliton formation in a fiber Bragg grating. *Optics Letters* 23: 328–330.

18. Eggleton, B. J., G. Lenz, R. E. Slusher, and N. M. Litchinitser. 1998. Compression of optical pulses spectrally broadened by self-phase modulation with a fiber Bragg grating in transmission. *Applied Optics* 37: 7055–7061.
19. Lenz, G., B. J. Eggleton, and N. M. Litchinitser. 1997. Pulse compression using fiber gratings as highly dispersive nonlinear elements. *Journal of Optical Society of America B*. 14: 2980–2999.
20. Lenz, G. and B. J. Eggleton. 1998. Adiabatic Bragg soliton compression in nonuniform grating structures. *Journal of Optical Society of America B*. 15: 2979–2985.
21. Strasser, T. A., P. J. Chandonnet, J. DeMarko, C. E. Soccolich, J. R. Pedrazzani, D. J. Digiovanni, M. J. Andrejco, and D. S. Shenk. 1996. Presented at *Optical Fiber Communications Conference*.
22. Sipe, J. E., B. J. Eggleton, and T. A. Strasser. 1998. Dispersion characteristics of nonuniform Bragg gratings: Implications for WDM systems. *Optics Communications* 152: 269–274.
23. Sipe, J. E., L. Poladian, and C. M. d. Sterke. 1994. Propagation through nonuniform grating structures. *Journal of Optical Society of America A*. 11: 1307.
24. Hill, K. O., B. Malo, F. Bilodeau, D. C. Johnson, and J. Albert. 1993. Bragg gratings fabricated in monomode photosensitive optical fiber by exposure through a phase mask. *Applied Physics Letters* 62: 1035.
25. Martin, J. and F. Ouellette. 1993. Novel writing techniques of long in-fiber gratings. *Electronics Letters* 30: 811–812.
26. Dong, L., M. J. Cole, A. D. Ellis, M. Durkin, M. Ibsen, V. Gusmeroli, and R. I. Laming. 1997. 40 Gbit/s 1.55 μm transmission over 109 km of nondispersion shifted fiber with long continuously chirped fiber gratings. Presented at *Optical Fiber Communications Conference*, Dallas, Texas.
27. Malo, B., D. C. Johnson, F. Bilodeau, J. Albert, and K. O. Hill. 1995. Apodized in-fiber Bragg grating reflectors photoimprinted using a phase mask. *Electronics Letters* 31: 223–225.
28. Sterke, C. M. d. and J. E. Sipe. 1994. Gap solitons. In *Progress in optics* 33, E. Wolf, ed. Amsterdam.
29. Eggleton, B. J., C. M. d. Sterke, and R. E. Slusher. 1999. Bragg solitons in the nonlinear Schroedinger limit: experiment and theory. *Journal of Optical Society of America B*. 16: 587–599.
30. Litchinitser, N. M., B. J. Eggleton, and G. P. Agrawal. 1998. Dispersion of cascaded fiber gratings in WDM lightwave systems. *Journal of Lightwave Technology* 16: 1523–1529.
31. Eggleton, B. J., C. M. d. Sterke, A. B. Aceves, J. E. Sipe, T. A. Strasser, and R. E. Slusher, 1998. Modulational instabilities and tunable multiple soliton generation in apodized fiber gratings. *Optics Communications* 149: 267–271.
32. Sterke, C. M. d. and B. J. Eggleton. 1999. Bragg solitons and the nonlinear Schroedinger equation. *Physics Review E*. 59: 1267–1269.
33. Eggleton, B. J., C. M. d. Sterke, and R. E. Slusher. 1996. Nonlinear propagation in superstructure Bragg grating. *Optics Letters* 21: 1223–1225.
34. Sterke, C. M. d., B. J. Eggleton, and P. A. Krug. 1997. High intensity pulse propagation in uniform gratings and grating superstructures. *Journal of Lightwave Technology* 15: 2908–2993.
35. Aceves, A. B. and S. Wabnitz. 1989. Self-induced transparency solitons in nonlinear refractive periodic media. *Physics Letters A*. 141: 37–42.
36. Peter, D. S., W. Hodel, and H. P. Weber. 1994. Compression of pulses spectrally broadened by self-phase modulation using a fiber grating: A theoretical study of the compression efficiency. *Optics Communications* 112: 59–66.

37. Linde, D. V. d. 1973. Experimental study of single picosecond light pulses. *IEEE Journal of Quantum Electronics* QE-8: 328–338.
38. Kuizenga, D. J. and D. W. Phillion. 1973. Simultaneous Q-switching and modelocking in the CW ND:YAG laser. *Optics Communications* 9: 221–226.
39. Stolen, R. H., J. Botineau, and A. Ashkin. 1981. Intensity discriminator of optical pulses with birefringent fibers. *Optics Letters* 7: 512–514.
40. Eggleton, B. J., R. E. Slusher, J. B. Dudkins, J. B. Stark, and A. M. Vengsarkar. 1997. All-optical switching in long-period fiber gratings. *Optics Letters* 22: 883–885.
41. Ahmed, K. A., B. J. Eggleton, H. F. Liu, P. A. Krug, and F. Ouellette. 1995. Simultaneous mode selection and pulse compression of gain switched pulses from a Fabry-Perot laser using a 40 mm chirped optical fiber grating. *IEEE Photonics Technology Letters* 7: 158–160.
42. Galvanauskas, A., A. Heany, and T. Erdogan. 1998. Use of volume chirped Bragg gratings for compact high-energy chirped pulse amplification circuits. Presented at the *Conference on Lasers and Electro-Optics*.
43. Williams, J. A. R., I. Bennion, and L. Zhang. 1995. Compression of optical pulse using self-phase modulation and linearly chirped Bragg-gratings in fibers. *IEEE Photonic Technology Letters* 7: 491–493.
44. Mollenauer, L. F., R. H. Stolen, and J. P. Gordon. 1980. *IEEE Photonic Technology Letters* 45: 1095–1098.
45. Winful, H. G. 1985. Pulse compression in optical fiber filters. *Applied Physics Letters* 46: 527–529.
46. Akhmanov, S. A., V. A. Vysloukh, and A. S. Chirkin. 1992. *Optics femtosecond laser pulses*. New York: AIP.
47. Mollenauer, L. F., R. H. Stolen, J. P. Gordon, and W. J. Tomlinson. 1983. Extreme picosecond pulse narrowing by means of soliton effect in single-mode fibers. *Optics Letters* 8: 289–291.
48. Chernikov, S. V., J. R. Taylor, and R. Kashyap. 1994. Experimental demonstration of step-like dispersion profiling in optical fibre for soliton pulse generation and compression. *Electronics Letters* 30: 433–435.
49. Mamyshev, P. V., S. V. Chernikov, and E. M. Dianov. 1991. Generation of fundamental soliton trains for high-bit-rate optical fiber communication lines. *IEEE Journal of Quantum Electronics* 27: 2347–2355.
50. Hill, P. C. and B. J. Eggleton. 1994. Strain gradient chirp of fiber Bragg grating. *Electronics Letters* 30: 1172–1174.
51. Eggleton, B. J., J. A. Rogers, P. B. Westbrook, and T. A. Strasser. 1999. Electrically tunable power efficient dispersion compensating fiber Bragg grating. *IEEE Photonic Technology Letters* 11: 854–856.
52. Lauzon, J., S. Thibault, M. J. and F. Ouellette. 1994. Implementation and characterization of fiber Bragg gratings linearly chirped by temperature gradient. *Optics Letters* 19: 2027–2029.
53. Sterke, C. M. d. 1998. Propagation through apodized gratings. *Optics Express* 3: 405–410.

54. Litchinitser, N. M., G. P. Agrawal, B. J. Eggleton, and G. Lenz. 1998. High repetition rate soliton-train generation using fiber Bragg gratings. *Optics Express* 3: 411–417.
55. Swanson, E. A., and S. R. Chinn. 1994. 23 GHz and 123 GHz soliton pulse train generation using two CW lasers and standard single mode fiber. *IEEE Photonic Technology Letters* 6: 796–799.
56. Gordon, J. P. 1983. Interaction forces among solitons in optical fibers. *Optics Letters* 8: 596–598.

Biographies

Benjamin J. Eggleton received his Bachelor degree with Honors in Physics from the University of Sydney in Sydney, New South Wales, Australia. His Ph.D. was received in the School of Physics and the Optical Fiber Technology Center in the Australian Photonics Cooperative Research Center, at the University of Sydney, in 1996. His doctoral research focused on linear and nonlinear effects in fiber gratings. He was awarded the 1998 Adolph Lomb Medal from the Optical Society of America for his work on nonlinear propagation effects in photonic bandgap. He joined the Department of Optical Physics at Bell Laboratories, Lucent Technologies, in Murray Hill, NJ, in 1996. In July 1998, he joined the Optical Fiber Research Department at Bell Laboratories, as a member of technical staff. His research interests include nonlinear optics, solitons, fiber optics, fiber gratings and photonic bandgap structures, all-optical switching devices, and dispersion compensation techniques in WDM lightwaves systems.

G. Lenz received his B.Sc. and M.Sc. in Electrical Engineering from the Technion-Israel Institute of Technology in 1988 and 1990, respectively. In 1995 he received his Ph.D. degree in Electrical Engineering from the Massachusetts Institute of Technology. In 1996 he joined Bell Labs as a postdoctoral fellow in the department of Planar Lightguide Circuits and in 1997 he became a member of technical staff in the Department of Optical Physics Research, where he has been ever since. His current interests include nonlinear optical materials for ultrafast all-optical switching, nonlinear phenomena in periodic structures, high-speed optical communication, and optical filters in WDM systems.

Natalia M. Litchinitser received her M.S. degree in Physics from Moscow State University, Moscow, Russia, in 1993 and her Ph.D. degree from the Illinois Institute of Technology, Chicago, IL, in 1997. She joined the Institute of Optics at the University of Rochester, in Rochester, NY, as a Postdoctoral Fellow in 1997. Her research interests include nonlinear and fiber optics, photonic bandgap structures, dispersion compensation in fiber-optic communication systems, short pulse generation, and compression.